On the Quantitative Tripartite Allocation of Atmospheric Vapor, Oqtav, by Oxygen 18

Mohamed Fahmy Hussein (profdrfahmy@cu.edu.eg)
Cairo University, Egypt https://orcid.org/0000-0003-0891-212X
Kamal Zouari
École Nationale d'Ingénieurs de Sfax, ENIS, Tunisie
Mohamed Anter
National Water Research Center, Egypt
Mariam Nosser
Cairo University, Egypt

Research Article

Keywords: Isotope hydrology, Atmospheric vapor mixture waveform, Atmospheric vapor mixtures (AVMs), Ternary AVMs model, Cairo, vapor mixtures, Nile Delta Apex vapor sources

Posted Date: September 10th, 2020

DOI: https://doi.org/10.21203/rs.3.rs-51992/v3

Abstract

The quantitative distribution of atmospheric vapor mixture, AVM, into three distinguished vapor end-members is lacking in the literature. This work fills such a gap. The isotope ratio, $d^{18}O_L$, of rainwater in Winter, and artificial condensates in Summer, gave the $^{18}O_V$ contents of local AVMs at temperature-dependent equilibrium, downtown Cairo city, Nile Delta apex. We used our models, SIMAM, CLAW, and SIGNALS to process the $d^{18}O_V$ and the commensurate specific humidity, S, values in several AVM data sets for determining the percent and mass contributions of three moisture origins and their temporal waveforms. The proportions and masses revealed Marine vapor dominance, followed by evapotranspiration. By far, the free Troposphere source showed a slight input. The quota of each constituent manifests a delayed waveform vs. AVM $d^{18}O$ influx, which shows a diurnal peak and a nocturnal tunnel. The moderate ET percent inputs in Winter, and by daytime, impose significant AVM ^{18}O enrichment. In contrast, the high Maritime vapor inputs in Summer, and by night, stand behind the depleted AVM ^{18}O content. The relationships between the mass input of each source and the AVM isotope ratio show significant dispersion for the negative trend of the diurnal-nocturnal Marine vapor in the two seasons. Such a high scattering is due to the mingling of northern wind-gust diurnal convection (marked by low Marine vapor input) and northern steady nocturnal advection (characterized by high Marine vapor input). Marine vapor waveform has a 12-hour time-lag by the intertwining of turbulent diurnal transmission, and steady nocturnal transport, through the long trajectory (180 km) from the Mediterranean coast to Cairo. In contrast, the relationships between ET mass input and AVM isotope ratio, on the one hand, and between the Troposphere vapor mass input and AVM isotope ratio, on the other hand, manifest low-dispersion positive and negative regressions, respectively. Such a low dispersion is due to the short transport pathway, the narrow range of the biological input (that increases only by daytime), and sharp Troposphere downdraft (moving northward in Winter but southward in Summer). Also, the ET waveform has a Zero-hour time-lag, like that of the Tropospheric vapor. Albeit the low S value of the Troposphere vapor pole, its impact on the AVM isotopic depletion is significant due to its extremely shallow ^{18}O content. The increase of the Tropospheric input at low AVM S values is related to regional drought, as expected. The high S values, of Marine and biotic origins, usually go with temperature apogees, especially in Summertime, as anticipated. The used models help in improving the time-series simulation of evaporation runs, since using seasonal $d^{18}O_V$ and S markers is better than using a snapshot. The ternary-vapor-source allocation procedure is a breakthrough in isotope hydrology. This thoroughly useful procedure will prove its ultimate benefits when the users get CRDS laser-controlled devices for the continuous measurements of the isotopic ratios in the local AVMs.

Introduction

The Planetary Boundary Layer, PBL, governs heat transfer, temperature fluctuation, wind blow up, and moisture transport with the air-mass flow in the atmospheric skin directly buoyant over land and ocean surfaces. The atmospheric vapor mixtures, AVMs, and temperature change are in close relationship to all the primary meteorological processes, including precipitation, evaporation, and transpiration.

The meteorological conditions of the Mediterranean basin are in sharp mismatch to that of the Great Sahara and acute contrast with the European continent in the north, and the cultivated lands of the Nile Delta in the southeast. The main features of the weather conditions prevailing in Cairo City, at the Nile Delta apex, are well known and entirely reported by recording and analyzing its typical parameters for long decades. However, hydrology research workers seldom publish the isotopic composition of precipitation (e.g., Zhang et al., 2020) and atmospheric vapor of the Mediterranean basin and for countries to the south in the region. This work is the first of its category for the 400 km^2 Cairo city urban zone, 180 km south of the seashore. This substantial urban zone is widely affected by the neighborhood of the vast rural counties of the Nile Delta, 20,000 km^2, to the north, and within earshot from the west, east and south territories surrounded by the extended Sahara terrains,

Despite the regionally prevailing excessive drought, governed in the first place by the Hadley Cell regime over the Great Sahara, Egypt may experience a few light precipitation events per year. A scarce violent deluge may also take place, however, one time per decade, via the advent of moist air-masses to accompany a sharp temperature gradient and the ordination of a temporary low air pressure that suddenly breaks down the over-heating regime ruling the permanent regional aridity for thousands of years in the Sahara. The perpetual zonal drought that dominates the climatic conditions in northeastern Africa and southwestern Asia is the primary result of the compression of huge air-masses downdrift from the Troposphere, Gasse, 2000, leading to powerful high-pressure cells, and subsequent adiabatic heating. This singular weather rupture leads to sporadic rainfall in Egypt. Such a rare weather breakage temporarily, but seldom, results in a swift but short adiabatic cooling period, of a few hours, and replace the everlasting adiabatic heating that dominates the vast Sahara territory for the last forty thousand years.

Studying the isotopic composition of the local AVM is a must for the interpretation of such isolated and exceptional precipitation events that would occur in the northeastern territory of the Great Sahara. More importantly, the AVM isotopic approach gives an essential tool to understand the dominant drought and quantifying its impact on the balance of the local and regional surface water used in the national production of food and other vital commodities.

A valuable, high-end application is to determine the quantitative distribution of the vapor sources that make up the local AVMs in Winter and Summertime. In meteorological hydrology, we need extensive information about the spatial and temporal moisture allowances in the air-masses over the agricultural regions affected by the freshwater scarcity that now extends, under the current human-made climate change, to Sub-Saharan Africa, Eastern Europe (Marchina, et, al. 2019), and Central Asia (Viviroli *et al., 2020*), not only the Sahara of the Arab countries and other nations in the Middle East.

The downstream Nile basin is a unique riverine system in its historical and current hydrological conditions in the dry and hot Sahara. The Nile Delta has seen an elaborate natural and human changes in the last few thousands of years. The interaction of old climate change and the human-made interventions (and their impact on the Nile downstream system) resulted in remarkable modifications in the water budget and land use in Egypt since the start of the written history, with aridity becoming more accentuated in the last two thousand years, Flaux et al., 2013. Such excessive aridity is a candidate to accentuate ahead from the present-day situation, Stephens, et al., 2020, and Khozyem, 2020. Besides, at present, there are intentional exterior dangers that threaten the Egyptian Nile inflow continuity, for the first time in history, by building dams on the Blue Nile, at the far head reaches, of such a river, old of six million years in Egypt, connected to the Blue Nile since 650 thousand y BP, after significant topographic and climatic changes in the northern and eastern African belts.

This work presents the first study of its kind in the field of the isotopic composition and quantitative distribution of three moisture sources in the local AVMs, at Cairo City, along with the change in the contribution of these vapor sources in Winter and Summer, primarily through the conjunctive use of the $d^{18}O$ data and the corresponding specific humidity of the AVMs. The purpose is not only to elucidate the internal mixing processes and to reveal its isotopic impact on the local AVMs isotopic signals but also to follow the trend of change in the contribution of each vapor source in the two seasons.

The details of daily and seasonal isotopic signatures of the local AVM can be beneficial for the experimental work on the estimation of the evaporative losses from local and regional surface water bodies under the steady and unsteady regimes. Such experiments are of prime interest for the follow up of the local and regional water budgets, Chun-Ta et al., 2006, Zhao et al., 2014, Benettin et al., 2018.

Besides, the present work makes use of the dynamic isotopic composition of the Summertime AVMs, on an hourly basis, for artificial condensates, instead of using average snapshot values in the long term, of about one day for each vapor sample, if the standard cryogenic vapor collection procedure was to follow. The high-resolution time scale, Helliker et al., 2002, is helpful for the precise simulation of the evaporation rates in virtual runs using a time-series set of data on a

computer, e.g., via the Hydrocalculator software, Skrzypek et al., 2015, and in the corresponding field experimental work using a Class-A pan. In the results and discussion item, we will see that the isotopic compositions of the local AVM pulses show a daily cycle (with distinct diurnal peak and nocturnal trough) that is to superimpose on the dominant isotopic enrichment in Winter vs. depletion in Summertime, for different reasons.

Furthermore, the lessons to learn from discovering the regime of the local AVM isotopic signals can be fundamental to regions as far as the Nile upstream reaches for the interpretation of the unique enriched isotopic composition of Nile water, as shown by the interactive diagrams in Fig 15 discussed later. In this context, the recycling of the evapotranspiration from the Nile upstream and downstream reaches, e.g., in the African tropical forest high lands and the Nile Delta, respectively, is to understand further using the stable isotope method as applied in the present work.

Moreover, the thorough isotopic information on the atmospheric vapor may later induce the incorporation of the isotopic signals of the AVMs into the international micro-meteorological data sets, since the isotopic composition of the AVMs is as energetic as the other meteorological parameters. Jointly with the satellite-based isotopic predictions, introduced by Isoscape, Ref, and Hysplit (Zhang et al., 2020). Such integration will promote the development of micro-meteorology and isotope hydrology since the current climate change is actively imposing additional shifts in different vapor sources contributing to the regional AVMs, especially ET recycling.

Methods And Theoretical Background

The modeling procedures used to get the contribution of three vapor sources to the local AVMs, and the waveforms of the AVMs' isotopic compositions, has recently appeared in another work (CLAW, SIMAM, and SIGNALS, in the press). We have started by the collection of artificial condensates in Summertime, and rainwater samples in Winter, over the last few years. The $d^{18}O$ ratios of the water samples were obtained on ABB LGR-ICOS Los Gatos Research tunable diode laser analyzer (Off-Axis Integrated Cavity Output Spectroscopy, OA-ICOS). The output provided by such an analyzer has an uncertainty of ±0.10 per mil for the measured $d^{18}O$ values vs. V-SMOW. Assuming the temperature-dependent equilibrium between each AVM and the corresponding liquid water phase, the isotopic composition of the vapor phase was calculated for each sample. The meteorological parameters were obtained using a Personal Weather Station data set, saved on a Laptop, in the water collection site. The validity of the temperature-dependent equilibrium is based on two characteristics of the study location. These characteristics are the high relative humidity, RH, and the low altitude (+46 AMSL) where minor deviations, caused by any artificial fractionation, would occur in opposite directions and cancel each other. Such opposition will favor diffusion, enhance isotopic equilibrium, and minimizes the systematic and random deviations from the equilibrium between the two water phases.

Isotopic equilibrium between the atmospheric water vapor and the liquid water phases is assumed in this article despite the recent isotopic disequilibrium claims (Mercer et al., 2020, and Penchenat et al., 2020). The authors advocating disequilibrium use monthly isotopic ratios at high altitude. In their works, they stand for disequilibrium via partial evaporation of the small raindrops (leading to a negative divergence) and evapotranspiration contribution (resulting in a positive shift). In contrast, we endorse isotopic equilibrium due to,

- High RH values that favor diffusive exchange and equilibrium between the two water phases.
- Low altitude (+46 AMSL) at middle latitude (30°N) for the study area where convective and advective processes are the convergence mechanisms. Isotopic equilibrium agrees with reported exceptions (e.g., Fiorella et al., 2019) for observations far from the Rayleigh model.
- Minor deviations are systematic in opposite directions (except for low RH values). Such deviations, however, are to verify in the future if we possess CRDS laser devices for the direct measurement of the isotopic composition of the local AVMs. However, we keep the equilibrium assumption as it will not perturb the used model.

Moreover, monthly precipitation sampling stands behind the claims against equilibrium (Mercer et al., 2020; and Penchenat et al., 2020). The hourly collection of the artificial condensates in Summer, however, supplies successful waveforms. If an acute deviation from the equilibrium between the two water phases existed, we would not be able to obtain our excellent observations. The hourly resolution is a valid method to obtain the isotope ratios. Long-term water sampling should result in claiming significant deviations from the isotopic equilibrium as bulk mixing of dispersed isotopic signatures may show disequilibrium between the two water phases while the natural processes govern the atmospheric moisture transport. Equilibrium exists, and it is quite a tremendous simple approach. However, if the research workers had their isotope ratios every month, they would conclude acute isotopic disequilibrium.

Accordingly, we calculated the $d^{18}O$ ratios of the AVMs, using the isotopic signatures of the collected liquid water samples, the temperature-dependent isotopic fractionation factors, and the meteorological parameters recorded at the time of each condensation and precipitation event. We have also calculated the absolute humidity (the mixing ratio, w, g per kg dry air) corresponding respectively to each AVM, by the time of every event, using temperature, t, RH, and barometric pressure, in August–Roche–Magnus formula of the Clausius–Clapeyron equation (not shown), and then we calculated the specific humidity, S, g per kg moist air,

$$S = [(w/1000)]/[1 + (w/1000)] * 1000.$$

Our isotopic distribution model (Sited Isotopic Mixing of the Atmospheric Moisture, SIMAM, in the press), gave the proportion of each of the three vapor end-members contributing to each AVM, Table 1. For each of the three vapor sources, we have *a priori* used an empirically verified isotopic signal, $d^{18}O$/V-SMOW‰, and a corresponding S value. The isotopic ratios and S values used for the three vapor origins were to verify and validate using the observed data-points as primary constraints applied to our model (Curvilinear Atmospheric Wedge, CLAW, in the press) as a framework that enclosed the AVMs' $d^{18}O$ data-points. Also, we sued our SIGNAL model to plot the waveforms of the AVMs' $d^{18}O$ values, and the three vapor sources contributions, concerning the time of each water sample collection. The SIMAM model was to run on Excel workspace, controlled by especial Macro. We adopted three moisture sources, namely, Tropospheric vapor, Marine vapor, and Evapotranspiration, ET. In this work, we call the Tropospheric vapor Sahara vapor for clarity and relevance. The three sources are conforming with weather conditions prevailing in Cairo city, where we have collected 74 samples of Summer condensates and Winter rainwater, Table 2.

Figs 1 to 12 give illustrations that classify into two types. The classification is to observe according to the parameter shown on the x- and y-axes. The grouping is also to see via the variations in the data in use in each diagram. The comments on these diagrams, and other helpful charts, Figs 13 to 22, make the heart of the discussion. The x-axis in Figs 1 to 12 either shows the S or the $d^{18}O$ values while the y-axis shows either the percent proportion or the Weight Parameter, WP, for a given moisture origin participating in the making up of each AVM. The weighted contribution (that we call the Weight Parameter, WP) has the same unit as S, as it is to calculate using the previously determined S value for each AVM, and the contribution of an individual vapor origin in the corresponding AVM

$$WP = (\text{individual percent contribution}/100) * S \text{ of the AVM}$$

This straightforward formula introduces the mass of the individual moisture source, instead of its proportion in the AVM. The WP value is handy praise not obtainable by any direct measurement as it offers a source-specific humidity-content for the concerned vapor end-member. With such individual absolute-humidity-parameter, we can tell, in Figs. 4, 5, 6, and 20, for example, how many grams of Marine moisture, or any other vapor source, is present in one kilogram of the moist air of each local AVM. The ternary mixing model, SIMAM, is to use first to obtain the percent contributions of up to three moisture sources in the local AVMs when the isotopic signals of these origins are known or assumed on some theoretical or empirical basis. The SIMAM model, however, is also to use for binary mixing, if required, by skipping the isotopic and humidity values of a third end-member vapor source in the used spreadsheet workplace and Macro.

[Please see the supplementary files section to view the tables.]

Results And Discussion

The Sahara moisture percent contribution is the lowest among the proportions of the three sources assumed to contribute to the AVMs in Cairo, Fig. 1., with a maximum value of 8% in Winter and 12% in Summertime. The Sahara vapor contribution is systematically higher in Summertime than in Winter. The negative relationship between the Saharan percent contribution and S reflects the role of the Saharan vapor source in the local drought, even in Winter. The high S values of the AVMs in Summertime represent a "lost chance" as the estival moisture cannot lead to precipitation due to the prevailing high temperatures. The hibernal intrusion of the Tropospheric (Saharan) downdrift also stands behind the abortion of precipitation in Winter. Rainfall events over Cairo and the Nile Delta are exceptional but may occur by a rare sudden breakage in the Hadley Cell regime governing the regional drought conditions in the southeastern Mediterranean basin. Rare precipitation events would occur, however, a few times per year, by the sudden advent of exceptional confrontation of external humid hot-stream with external cold air-masses. Infrequent significant precipitation may also take place, a few times per decade, *via* the inception of a regional deep and vast depression cell that leads to sharp adiabatic cooling, as the one called "Dragon" shower of 12-14 March 2020. Compared to the contributions of the Marine vapor and ET concerning S, shown in Figs. 2 and 3, the relationship of the Sahara vapor contribution with S, Fig. 1, shows a salient low dispersion in the two seasons. This behavior reflects the consistency of the Tropospheric (Sahara) downdrift that produces adiabatic heating the year-round.

Fig. 2 is showing that the Marine moisture contribution dominates the scene in Winter and Summer in Cairo AVMs, as expected. In both seasons, the percent contributions and S of this northern moisture source show a wide range of values and faint positive trend of x and y variables in Summer vs. a weak negative trend in Winter. The relationship between the two variables is not significant since dispersion is considerable compared to that of the Sahara vapor contribution behavior shown in Fig. 1. Such considerable scattering reflects the oscillation of the Marine source input in a prominent daily cycle with the wind gusts passing southward, especially in Summertime, Fig 23. Few Summer data-points, however, show lower Marine contribution than most of Winter data points. These few points correspond to some condensates collected in the Spring of the year 2019, not in Summertime (S values are known to be sometimes lower in Spring than in Winter). Recently, research workers (Bonne et al., 2019) have recommended that relative humidity and sea surface temperature (not wind speed) only are the two variables that control deuterium excess of the Marine vapor within the PBL.

The attitude of the ET moisture input vs. S in Cairo AVMs, Fig. 3, works as a vertical mirror image of the behavior of the Marine vapor input vs. S, shown in Fig. 2. The high dispersion of the relationship between ET contribution and S in Winter and Summer reflects the variation in the biological activity of the Nile Delta vegetation in response to the current S values in the two seasons. However, a bulky scatter appears at a higher S level in the hot season and shows a weak negative trend, compared to a significant positive regression with less dispersion for the cold season. The opposite trends are expressions of different ET fluxes and as byproducts of the Marine source dominance. The diurnal temperature increase,

in the two seasons, however, induces higher ET signals vs. the nocturnal ET fading that starts by evening. On the contrary, the ET contribution signal is showing low dispersion in Fig 9 for its relationship with $d^{18}O$ of the AVMs, in the two seasons, with a steeper regression in Winter. Such a steep regression is related to the Winter crops that produce low ET fluxes, isotopically enriched, in Winter.

The relationships of the Sahara vapor WP with S Fig. 4 show the same behavior of the relationships of the Sahara percent contributions with S, Fig. 1, except the linear regressions with a slightly larger negative slope, and lower locus, in Winter than in Summertime. The higher WP values in Summer reflect stronger downdrift of Tropospheric (Sahara) air layers in the hot season. Albeit the remarkably low WP values of the Sahara source in the local AVMs in the two seasons, their isotopic impact on the isotopic ratio of the AVMs is sharp due to the profound isotopic depletion in the Sahara vapor.

Fig. 5 is showing the relationships of the Marine moisture WP with S. The behaviors of such relationships sharply differ from the relationships of the percent contributions with S, Fig. 2, both for Winter and Summertime. Here, the two seasons show positive linear regressions and much less dispersion. The WP-S regression has more significant R^2 value in Summer than in Winter; 0.7702 and 0.4398, respectively. The higher WP levels in Summer agree with the visible dominance of the northern windblown to Cairo City in the hot season, Fig 23. Also, the highest S value in Summer is almost double the highest S value in Winter, due to significant Marine vapor southward flux in Summer. The remarkable estival WP values for the Marine vapor source lead to an accentuated isotopic depletion in Cairo AVMs in Summertime.

The ET WP relationship with S, Fig. 6, is like the ET percent contribution relationship with S, Fig. 3, except for the signs of the two regressions. The Summertime data-points, however, show much dispersion in Figs 3 and 5. The WP ranges of ET for the hibernal and estival seasons are comparable and reflect the permanent biological activities in the cultivated Nile Delta lands. These activities produce about the same absolute ET moisture despite the different ET fluxes in the two seasons. This piece of information is precious since it reveals the moisture-distribution that the percent contribution may hide. The wide WP range of the vegetative source in the two seasons is a direct reflection of the weather conditions and the cropping pattern in the Nile Delta since ET is absent by night, something that accentuates the diurnal signal of ET WP in the two seasons. However, the hibernal ET WP data-points appear at a lower S position and show much more significant regression than the estival ET WP data-points.

The Sahara vapor percent contribution in relationship with $d^{18}O$ of the AVMs, Fig. 7, is higher in Summer than in Winter, but both show high scattering. Compared to the behavior of the relationships of both the percent contributions, of the Marine moisture and ET, with $d^{18}O$, shown in Figs 8 and 9, the Sahara vapor source percent contribution concerning $d^{18}O$ shows a notably high dispersion. This chaos reflects not only a daily cycle but, more importantly, the permanent presence of such drought source in Cairo AVMs the year-round. However, Figs. 1 and 4 show that the percent contributions and WP values for the Saharan vapor concerning S have extremely low dispersions and visible negative regressions in both Winter and Summer. However, Fig. 7 also illustrates that the Sahara vapor source percent contributions are showing up at all the observed $d^{18}O$ range of the local AVMs in both Winter and Summer. Nonetheless, such a vapor source has a slightly higher contribution at the moderate and low ^{18}O contents of the local AVMs in Summer vs. its low contributions at the full $d^{18}O$ range in Winter. The last statement could, however, be an artifact produced by the mixing process of the regional vapor sources. Otherwise, there is a seasonal change in the $d^{18}O$ or S value of the Sahara pole; a change that nobody can verify for the time being.

The percent contribution of the Marine vapor concerning $d^{18}O$ of the AVMs, Fig. 8, has a wide range of values that are almost comparable for Winter and Summer (few data-points to the left-hand side correspond to Spring, not to Summertime). Compared to the behavior of the relationship of the percent contribution of the Sahara vapor with $d^{18}O$ shown in Fig. 7, the corresponding relationships for the Marine vapor in Fig. 8 are showing low scattering and negative

linear regressions with steeper slope (-0.1504) in Winter than in Summer (-0.0872). This trend reflects the Marine vapor dominance the year-round, and that it has extensive daily cycles that are unequally partitioned between the daytime and nighttime. The high Marine contributions in the two seasons, however, are associated with the isotopically depleted AVMs. The Marine vapor source negative regressions with $d^{18}O$ for the two seasons are opposite to the ET positive regressions shown in Fig. 9 as if the opposition is a vertical mirror image.

Fig. 9 is showing that the ET percent contribution with $d^{18}O$ values of the AVMs is slightly higher in Winter than in Summertime (except for the few Spring data-points shown to the right-hand side below the regression line). Both relationships, however, have a significant positive regression. Compared to the behavior of the percent contributions of the Sahara and Marine vapor, Figs 7 and 8, respectively, the ET data-points have very low dispersion. Such positive trends reflect the permanent presence of the ET vapor source the year-round and thanks to its diurnal pulse and nocturnal fading. Higher ET percent contributions are associated with isotopically enriched AVMs in Winter (keeping the few Spring data-points excluded). However, the last statement could be an artifact of the mixing process of the three vapor sources if the isotopic composition of the ET pole was not further enriched in Winter but more depleted in Summertime. The steeper positive ET regression with $d^{18}O$ in Winter shown in Fig 9 agrees with the ET high flux released out from the Nile Delta crops in the cold season, and such a high hibernal ET flux is more than expected for the cold season. However, the last statement could be an artifact of the mixing process of the three vapor sources. Otherwise, the isotopic composition of the ET vapor pole would have a remarkable enrichment in Winter and more depletion in the Summertime. Such an isotopic shift is to verify in the future. Nonetheless, the isotopic depletion of some data-points of the AVMs in Summertime may result from the isotopically depleted ET flux of a Summer crop (e.g., Corn). However, the situation is so beautifully complex to be justified by a single crop criterion since other data-points show visible isotopic enrichment in Summertime, as shown in Fig. 14 bottom corner diagram. The interactive diagram in Fig. 15 shows that the decrease of ET contribution in Summer is responsible for the significant isotopic depletion in the estival AVMs (as the higher contribution of the Marine vapor source is the real reason for such isotopic depletion in the hot season). The decrease in ET contributions in Summertime is a byproduct of the estival sharp increase in the Marine vapor source contributions. Thus, the Marine source is actively transferring its depleted isotopic fingerprint to the AVMs, preferably in Summertime. As the available data is showing ET contributions in the two seasons, we may look at the point at 30% in Summer in Fig 14. The ET flux from the Nile Delta (*via* the ratio of the ET flux to the applied irrigation water) is about 35 BCM in Summer. The total AVMs in the Nile Delta in the hot season would amount to 100 BCM, with 65 BCM mass directly flowing out from the northeastern Mediterranean basin, and the rest is from the ET. Such 100 BCM moisture corresponds to the approximate value calculated using the regional specific humidity calculations reported elsewhere (Specific Humidity Calculator_7_SUMMARY_OF_MEAN_VALUES_and_Project Operation Zone_4, in the Folder Water Generation Project_Specific Humidity in the Folder Hydro.)

The Sahara WP values in relationship with $d^{18}O$ of the local AVMs, Fig. 10, is systematically higher in Summer than in Winter. However, the Sahara WP values are showing higher dispersion in Summer than in Winter. The distribution of the data-points for the two seasons over the full $d^{18}O$ range is related to the omnipresence of Tropospheric downdrift the year-round. Such drought effect occurs e without correlation with the $d^{18}O$ content of the AVMs. However, in Summer, there is a data-point cluster of this moisture source concentrated at the moderate and depleted isotopic signatures of the local AVMs.

The Marine WP values Fig. 11, is much higher in Summer than in Winter. The data-points for the two seasons, however, show high scattering. Compared to the behavior of the WP values of the ET source, Fig 12, the Marine WP values are showing extensive dispersion, especially in Summer, with non-significant regression in the two seasons. The reason for the high dispersion is that the Marine vapor fluxes experience periodic diurnal and nocturnal change between convection

and advection, respectively. However, the Marine vapor data-points visibly show some clusters at the moderate and depleted isotopic compositions of the AVMs in Summertime.

Fig. 12 is showing that the relationship of WP values of the ET source with $d^{18}O$ of the local AVMs has significant positive regressions in the two seasons, with a slightly steeper slope, 0.9617, in Winter than in Summer, 0.9539. Compared to the behavior of the corresponding contributions of the Sahara vapor and the Marine vapor, Figs. 10 and 11, respectively, the relationships of ET WP with $d^{18}O$ is showing very low dispersion and significant positive repressions for the two seasons. The two configurations reflect the perpetual release of diurnal ET flux the year-round, but with more impact on the AVMs isotopic enrichment in Winter.

To this extent, we show what happens to the contributions of three vapor sources when we used one fixed value for the isotopic composition of each vapor source and two values for S, one for Winter and the other for Summer. For more practical purposes, one refers to these two values as exhalation in Winter, and inhalation in Summer to consider what happens when dealing with the "inhalation" of the S values in the Summertime vs. the "exhalation" that occurs in Winter. By the term "inhalation," we mean the significant increase in the S value for each vapor origin in Summertime, in contrast to the term "exhalation," which means a remarkable decrease of S value for each vapor origin in Winter, Fig 21. Such changes in the S values correspond to the acute change in the temperature and RH in the two seasons. To keep things simple, we assumed, however, that no change in the isotopic composition of the three vapor sources takes place. The reduction of the specific humidity in Winter will result in the shrinkage of the curved wedge shown by the CLAW model, Fig 21, and consequently, the shift in the percent contributions, and the WP values, calculated by the SIMAM model, for the three vapor sources contributing to the AVM. Other users may, however, appraise for making some change in S and $d^{18}O$ values for the three vapor sources. Such changes are to introduce by the user as required for his experimentation.

Fig. 13. The increase of the Marine vapor source percent contribution (top-left diagram) leads to isotopic depletion in the local AVMs. In contrast, progressive AVM isotopic enrichment goes with ET source percent contribution increase (middle-left diagram). In Summertime, the Marine vapor source contribution (top-right diagram) increases at high S values while the ET source contribution (middle-right diagram) increases at low S values. Under the hot Summertime weather conditions, the cultivated crops in the Nile Delta react by releasing higher ET flux, especially when the S values are low. The high ET contributions at the low S values in Summertime is due to high ET fluxes from the Nile Delta vegetation under the apogee temperatures prevailing in the hot season. In contrast, the lack of trends in Winter, for both the Marine and ET contributions with S, reflects apparent moisture stagnation in the cold season due to the steadiness of the northern wind replaced by the southern wind that partially resists the ET signal transmission to Cairo city in the cold season, Fig 23. The relationship between the percent contribution of the Sahara vapor source with S values (bottom-right diagram) shows a curvilinear increase with S decrease in the two seasons, with higher estival contributions of the Sahara moisture at higher S values, as in Fig 1. This observation reflects the active role of the Sahara vapor source in the regional drought the year-round. On the contrary, the Sahara moisture source has no definite relationship with $d^{18}O$ of the AVMs (bottom-left diagram) the year-round, as in Fig 10.

Fig 14. The negative relationship between ET percent contribution and S (top left diagram) is showing lower ET contribution in Summer than in Winter despite the high ET flux in the hot season. This odd trend is an artifact (byproduct) of the massive impact of the Marine vapor contribution increase in Summertime (top right diagram). In contrast, the bottom diagrams show the inverse trends for the relationship between the ET and Marine contribution, on the y-axis, and $d^{18}O$ ratio, on the x-axis. The left bottom diagram is showing a positive relationship between ET contribution and $d^{18}O$ in Winter and Summer. The tight bottom diagram shows a negative relationship between the Marine contribution and $d^{18}O$ in the two seasons. The higher Marine vapor contribution in that diagram shows a data-point cluster at the isotopically depleted atmospheric vapor mixtures in Summer. Despite the observations mentioned above, the isotopic compositions of the AVMs almost cover the full $d^{18}O$ range in the two seasons. ET contribution increase associated with dryness and

isotopic enrichment (in Winter and at the low S value in Summer). In contrast, the increase of the Marine contribution is associated with wetness and isotopic depletion of the AVMs (in Summertime).

Fig. 15. Interactive diagrams are based on the left bottom diagram shown in Fig 14. These four diagrams are to run in Excel to show the impact of the different isotopic compositions and percent contributions of the used three vapor sources on the isotopic composition of the local AVMs. These water vapor mixtures visibly become more isotopically depleted in Summertime at the low percent contribution of the ET vapor source when the Marine vapor contribution is at maximum. Besides, the Sahara vapor end-member has a higher contribution to the Summertime than Winter AVM. Also, the estival increase in the Sahara vapor proportion, to 10-12% in Summer, partially leads to the isotopic depletion in the AVM in the hot season (black square in the left bottom diagram). Albeit the shallow S values for the Sahara vapor origin, its extreme isotopic depletion stands behind its perceivable impact on the isotopic composition of the local AVMs, especially in Summertime. The visible hibernal isotopic enrichment of the AVM is the direct result of the high ET vapor source contribution in Winter (the black square in the left bottom diagram shifts upward).

The water liquid phase that would condensate from an AVM, with-10 per mil for $d^{18}O$, will have the $d^{18}O$ value of about 0 per mil for the obtained precipitation. This example is of primary importance for the interpretation of the isotopic ratios of the Nile water at the river middle African head reaches. Assuming a dominant ET recycling origin, for the significant precipitation events that make most of the runoff that goes to the River Nile, at its up reaches, and assuming -10 per mil for $d^{18}O$ of the AVMs at the river head reaches, and 0 per mil for $d^{18}O$ for mid-African precipitation, the runoff water that goes to the river course would show $d^{18}O$ of about +1 per mil, or so, in the African rainforest heights upstream. Then, the river water gets more isotopically enriched by evaporation as it flows across the long northward pathway that finally reaches the flat downstream terrains of Egypt. In contrast, if, by quite an argument, the condensation of a dominant Ocean water vapor source was, instead, to mostly form the primary precipitation events at the Nile upstream territories, the middle-African runoff that goes to the river would be marked by accentuated isotopic depletion, which is not the case. The isotopic enrichment of the Nile water, at its head reaches, visibly reveals the dominance of ET recycling, at the upstream territories (Ref), and is to attribute to massive ET flux of the dense tropical rainforests. Any widescale clearance of the tropical forests in the middle African territories will catastrophically diminish the Nile water discharge towards the downstream countries. The interactive diagrams, shown in Fig 15, supply an excellent tool for the interpretation, not only of the isotopic composition of the AVMs downtown Cairo city but also for understanding the enriched Nile water isotopic composition in the upstream mountainous regions, as we have just explained in the last few sentences.

Moreover, we believe that the accelerated deforestation in tropical Africa (Neef, 2020) will lead to diminishing the ET proportion in the African AVMs that induce precipitation at the Nile upstream countries. High ET recycling in the Nile's head reaches stands behind the enriched isotopic composition of the upstream river water, Fig. 15. As such, a significant depletion in the isotopic signature of the Nile water will visibly be due to the substitution of a fraction of the ET origin by the Ocean vapor in the rainforest tropical African territories due to unfortunate massive deforestation. Hundred years ago, the rainforests territories were covering about 14% of the total land worldwide, but today it is only about 6%, and the human activity has removed about half of the tropical rainforests.

Fig 16. The relationships of the ratio of the contribution of ET vapor source to that of the Marine vapor with the isotopic composition (left-hand side diagram) and the S values (right-hand side diagram) for the AVMs show two inverse regressions and seasonal fingerprints, 1) ET to Marine ratio is increasing with the enrichment in ^{18}O (left diagram). 2) ET to Marine ratio is decreasing with the increase of the S values (right diagram). The horizontal line shown at the y-axis value of unity, in both diagrams, is to use to follow the deviations from the equity of both vapor sources contribution.

Fig.17. The four Korean-style diagrams shown in this figure illustrate the differences between the ternary and binary mixing models and what they have in common. The ternary mixing charts (top charts) are more successful than the

binary blending (bottom charts). The top sketches are showing the relationship between the $d^{18}O$ and S values of the AVMs s in the Nile Delta apex in Winter (left charts) and Summer and Winter together (right charts). S no account can ignore the ET contribution in the atmospheric moisture over such a vast delta, the ET source participation was to include in the ternary mixing model. The ET vapor source has the effect of dragging the data-point towards the top right corner in each of the top diagrams. The position of the literature data-points, taken from Gat et al., 1995, for the atmospheric moisture over the eastern Mediterranean Sea, January 1995, is astonishing. Gat data-points are lying nearby the top left corner, in the four diagrams, i.e., to the left side of our Winter data-points, for Cairo city. The surprising Gat data-points positions reflect not only the extreme drought under the impact of the shallow moisture content of the Sahara vapor but also show the presence of an ET component in the vapor samples collected using a standard cryogenic procedure in Winter of the year 1995. What Gat and co-workers have sampled and measured was not a pure Marine moisture, but mixtures of Marine atmospheric vapor affected by the Tropospheric downdrift over the Sahara, plus ET component from the European continent. Drought appears, on the x-axis, on four diagrams, via the low S values (top charts) and the mixing ratio, w, values (bottom graphs). Comparatively, Gat's data-points configuration indicates that even in Winter, the air masses over the Nile Delta apex at Cairo city have higher humidity contents than that of the air-masses over the open eastern Mediterranean water surface. Unfortunately, Gat and co-workers have not reported any isotopic or humidity data for the east Mediterranean basin in Summertime. However, we may assume that the isotopic composition of the atmospheric moisture over the eastern Mediterranean will stay constant the year-round (and show the same range of values as that of Gat's Winter isotopic contents). Only the S and w values will significantly increase in Summertime in this Marine basin. Gat data-points will, virtually, move (on an oblique line with the same trend as that of our data-points for Cairo city) to the right-hand side bottom corner of the four diagrams if Gat and co-workers have also sampled the atmospheric mixtures over the eastern Mediterranean in the Summertime of the year 1995, as they did in Winter of the same year. Nevertheless, Gat's virtual data-points in the new position, for such an imaginary Summertime campaign, will appear in the two diagrams above our Cairo data-points and the oblique binary mixing line of the Marine and the Sahara vapor. The presence of our data-points below the Gat imaginary estival campaign might indicate that our isotopic compositions for Cairo city have isotopic depletion compared to the eastern Mediterranean basin vapor. What, then, would be the meaning of such isotopic depletion in our data-points? Would the assumed depletion in our data-points indicate the impact of climate change (namely, via air temperature increase) over during the 22-24 years between 1995 (Gat's sampling date) and2017/2019 (dates of our work)? The answer is no. The reason for such a net negative response is that any significant increase in air temperature will lead to a decrease in the value of the equilibrium fractionation factor, and this leads to a more enriched isotopic composition for the AVM corresponding to our collected liquid-phase water samples. In contrast, we are looking for a plausible reason for the thought depletion in our ^{18}O values (of the local AVMs assumed in equilibrium with the liquid phases that we have collected in Winter and Summertime) compared to the eastern Mediterranean vapor isotopic composition. The sole reason for negating the depletion discrepancy in our data-points is the mixing dynamics of three vapor sources, including the ET component as an important isotopic enrichment controller in the regional AVMs. Such a biological controller governs the positions of our data-points shift towards the top right corner in the four diagrams, even if the contribution of the ET source is not significant. We conclude, then, that Gat's vapor samples had a substantial ET component diffused from the European continent, and he has not reported such a potential component over the open seawater surface of the eastern Mediterranean basin. If Gat's vapor samples had not any ET component, his data-points would precisely show up on the binary mixing line of the Marine and the Sara sources in the four diagrams, not above such a line. This argument says that Gat data-points are more enriched than expected from the simple binary mixing between the Sahara and the Marine vapor sources. Such enrichment is certainly due to the impact of the continental ET component in Gat's vapor samples. Noteworthy also is to mention that the limits of our experimental data-points for the local AVMs have governed the isotopic composition and specific humidity for the Marine vapor source. However, the compositions of our three vapor sources are tentative and may be subject to seasonal shifts but never to the extent to force our Marine pole to appear in the position and place of Gat's Marine vapor data-points. When the Cavity Ring-Down Spectroscopy, CRDS, devices provide full isotopic data by the continuous and direct

measurement for the local AVMs, such controversy may get to an end. However, we are not the only research workers who mention critics of Gat data. A preprint, unpublished discussion paper (Cox et al., 2012) has already contended issues in the d-excess values for the eastern Mediterranean surface water reported by Gat in 1996 for his 1988/89 data and attributed such a discrepancy to faulty isotopic measurement by Gat teamwork.

Fig. 18. The ternary Piper diagram is showing the contributions of the three vapor sources composing the local AVM data-points. Our data-points are mostly aligned close to the right-hand side of the Piper triangle. The right-side is a binary (Marine and ET) mixing line. The Sahara vapor contribution increase drags the data-points to the left-hand side, towards the Piper inner space. Such a triangle supplies complementary information to add to the data-points orientation pointing towards the top corner of the Korean-style space to the right-hand side of the Sahara-Marine binary mixing line (top diagrams in Fig 17). The Korean-style chart shows the binary mixture of the Marine and Sahara vapor, where ET contribution increase triggers the data-points to the top right corner. The Korean style space is superior to the Piper triangle as we do not need to know the percent contribution of the three vapor sources in each AVM. However, the Piper triangle is superior as it shows the percent input of each vapor source. Piper triangle, however, would fail if the contribution of one of the three vapor sources was not available. Nonetheless, we have plotted Gat's data-points of January 1995 (Gat et al., 1995) on the Piper diagram, using the binary Marine and Sahara vapor mixing, just for illustration purposes, via ignoring the ET component data in SIMAM model and Macro. The ET component was to ignore in Gat's data-points processing for this purpose. The reason is that no calculation is possible via our SIMAM model for the Gat-data-points using his isotopic ratios and S values as we do not know the $d^{18}O$ and S values to use for the ET source contributing to Gat's data-points. Still, we may assume it, in other work, as being a continental (European) ET component for which we may find the corresponding isotopic and humidity data in the literature. However, the most critical problem in Gat isotopic data is that each of his collected vapor samples was to obtain in about one day, and thus the provided temperature and RH data were also mean values over time and space. This obstacle is challenging due to the bulk nature of Gat's isotopic and meteorological data in terms of the long time needed to collect each vapor sample via the standard cryogenic vapor procedure. The long time required for collecting each vapor sample means that the isotopic ratio for each vapor sample was an average value to report overtime and on the ship navigation trajectory. This situation leads to unavoidable irregularities as the isotopic ratio of the atmospheric vapor, and the corresponding meteorological data will change every hour. In contrast, our samples have an excellent temporal resolution of one hour at one location. However, we may assume that the visual projection of Gat data-points would show a virtual ternary mixing configuration that indicates about 15% ET contribution, 10% Saharan vapor component, and 75% for the proper Mediterranean vapor source, as a first approximation. Albeit its strange shortages, Gat data reflect that each of his vapor samples is to primarily represent a mixture of at least two vapor sources, namely the Marine vapor and the Tropospheric moisture (Sahara vapor). This observation also means that there is no isotope and humidity data possible for any pure Marine vapor pole over the eastern Mediterranean Sea. The isotopic and humidity data for a pure Marine vapor source would never exist over such a semi-closed sea. The Mediterranean, contrary to the open oceans, unavoidably gets the impacts of the continental moisture fluxes, out from the European, Asian, and African continents, via the wind activity. Accordingly, we are right in assuming the isotopic composition and specific humidity reported in this work for the theoretical Marine vapor source as constrained by fitting Cairo city data-points by the Macro of SIMAM model. If the late statement is not the last word in the quantification of the isotopic composition of the atmospheric vapor of the region, it offers an outline direction on the long road. No atmospheric vapor source is a "pure" vapor source No single statement, however, can settle every conflict in that issue without using an hourly resolution for the continuous and direct measurement of the isotopic composition of the local AVMs using the adequate CRDS devices. Moreover, the satellite Isoscape isotopic model could not fill such a gap.

Fig. 19. The top diagram is showing the opposite trends of the two dominant vapor sources, the Marine vapor (circles) and ET (triangles) for the relationship of the $d^{18}O$ values of the atmospheric vapor mixtures (on the y-axis) with percent

contribution of each source in the AVM (on the x-axis) in Winter (blue symbols) and Summertime (yellow symbols). The contribution of the Sahara vapor, shown by small rectangles at the left-hand side of the top diagram, has minimum values that rarely exceed 10%. The low ET contributions are associated with the isotopically depleted AVMs in both seasons, the moderate ET contributions associate with the moderate to high isotopic enrichment of the AVMs in Winter, and the high ET contributions associate with the isotopically enriched AVMs. The high Marine contributions associate with the AVMs isotopic depletion in Summer. The association of the extremely high Marine vapor contributions with the extreme depletion of the AVMs puts a useful constraint on the isotopic composition to assign to the theoretical "pure" Marine vapor source of the eastern Mediterranean Sea. The bottom diagram is showing a set of quasi-linear relationships between the S values (on the y-axis) and the percent contributions on the x-axis. The S value shown on the y-axis is not the S value for the AVM but the S value for each of the three vapor sources in the mixture, as calculated by SIMAM Model. The ET moisture shows low to moderate contributions at low to moderate specific ET_S values in Winter, while both variables slightly increase in Summertime. The Marine moisture source shows moderate to high contributions at moderate to high S Marine values in Winter while showing moderate to very high contributions associated with moderate to extremely high Marine_S values in the Summertime.

Fig. 20. The diagram shows that the high ET WP values, on the x-axis, associate with highly enriched isotopic signals of the AVMs (on the y-axis) in the two seasons, with steeper regression in Winter. In contrast, the chaos of the WP relationship with the $d^{18}O$ values of the AVMs is to observe for the Marine vapor source, especially in Summer (Risi et al., 2020). The low WP values for the Sahara vapor source cover the full range of the $d^{18}O$ range of the AVMs, with a slight increase in Summer. The considerable variation of the WP distribution for the three vapor sources with the isotopic signature of the AVM is a direct expression of the aerodynamic processes at the Nile Delta apex.

Figure 21. Two curved wedge frameworks produced by the CLAW model (three blue curves for Winter and three red curves for Summertime) including our data-points for Winter (blue and black squares) and Summertime (red circles and red spots). The Mediterranean data-points (Gat Jan 1995) appear as purple void squares, to the left-hand side, inside the blue "Winter exhalation" framework but outside the red" Summer inhalation" framework. The difference between the data-points distributions in Winter and Summer is visible inside the two frameworks. However, the diagram setup is for the relationship between $d^{18}O$ and S values for the AVMs, while Fig 20 shows the three vapor sources composing the local AVM using the SIMAM model for the relationship between $d^{18}O$ of the AVMs and the individual WP values for each vapor origin. It is astonishing to remark that S values in Cairo AVMs in Summertime exceed S values in the AVMs at the Southern Amazon basin.

Figure 22. The daily evaporation rates, downtown Cairo city, for the years 2018, 2019, and 2020. The Winter season is showing a low evaporation rate plateau, with an average of 4 mm per day, while the average of the estival plateau is at 12 mm per day. The Spring season shows an ascending evaporation rate trend (primarily due to temperature increase under low RH values), with sharp oscillations between 6 and 16 mm per day, that may reach 22 mm per day under the impact of hot and dry air-mass surges. Autumn is showing a visible descendent trend, via the rapid decrease in temperature while the RH values are still high.

Figure 23. Guided by the shown wind rose, we assume a mean northern wind speed of 5 km/hr. This speed will impose a 36-hr delay on the diurnal and nocturnal Marine isotopic and humidity signals to arrive at Cairo across 180 km (the distance between the Mediterranean coast and Cairo city). The ET vapor source has a 24-hr delay for its diurnal isotopic and humidity signals to cross a 120 km distance between a point in the middle of the northern sector of the Nile Delta (i.e., 60 km to the south of the Mediterranean coast) and Cairo city.

Figure 24. The Time-controlled dynamics, for the change in the percent contributions of the three vapor sources making up the local AVM, at different geographic keystones to the north of Cairo, namely, 1, at the Mediterranean coast, i.e., +180

km, 2. at +120 km, 3. at +60 km, and 4- downtown Cairo. The top diagram is showing elusive horizontal mirror-image for the Marine, and ET, percent contributions downtown Cairo (large blue and green squares, respectively) as the Marine %input increase by nighttime in Cairo is visibly counter-intuitive. Such nocturnal Marine contribution increase in Cairo is an artifact imposed by the time-lag caused by wind direction, trajectory, and speed since the Marine windblown mostly starts at the Mediterranean coast. Compared to the Marine signal, the ET signal trajectory is shorter (considered here at +120 km, i.e., at the north of the central cultivated lands of the Nile Delta). The diurnal increase in the ET source percent contribution is normal behavior as transpiration fades out by nighttime. The behavior of the Sahara vapor percent contribution (small void red squares, bottom diagram) is like that of the ET source percent contribution as the Sahara signal also has a short trajectory (considered here at +120 km), and the active diurnal wind helps in its transmission to the capital mostly by daytime. Assuming diurnal and nocturnal northern wind speeds of 8.88 and 3.75 km per hour, respectively, the northern diurnal wind needs 1.69 days to reach Cairo while the nightly northern wind needs four days. Alternatively, for simplifying, we consider a mean speed of 5 km per hour for the northern wind the year-round, and we change the distances of the initiation geographical keystones from Cairo for both the Marine and ET percent contribution signals. The top left corner labels marked as +180, and +60 km (top diagram) show two initiation keystones for the Marine vapor source, one at +180 km to the north of Cairo, i.e., at the Mediterranean coast, and the other at +60 km, i.e., inland in the Nile Delta nearby the capital. The percent contribution of the coastal Marine vapor source (at +180 km) will be subject to acute modifications as it travels southward to Cairo. It will reach the capital after 36 hours, i.e., with a 12-hour time-lag, while the ET source signal, initiated at the +120 km keystone to the north of Cairo, will have no time-lag, as it takes 24 hours to reach the capital when transported by the same northern wind speed of 5 km per hour. The notable time-lag for the Marine percent contribution will lead to the significant dispersion observed in Figs. 11 and 20 for the relationship between $d^{18}O$ and WP of the Marine vapor source. Such a high scattering (Risi et al., 2020) is due to the active blend mingling of the Marine vapor controlled by the dominant northern wind activity. The Marine vapor is isotopically enriched, and has higher WP values, by daytime; still, the inverse is right for nighttime. These differently marked isotopic-humidity signatures of the Marine vapor source by daytime and nighttime will actively mix along with the signal trajectory southwards, and such blending will cause the observed high dispersion for the relationship between $d^{18}O$ and WP of the Marine vapor in Cairo downtown, plot Figs. 11 and 20. There is no such scattering for the relationship between $d^{18}O$ and WP for the ET source since the ET signal goes only by the daytime. At the coast, there is no ET component, i.e., the local AVM is just a binary mixture of the Marine and Tropospheric vapor sources. It is noteworthy to observe the increase in the percent contributions of ET and Sahara vapor sources by daytime vs. the decrease in their nocturnal contributions. In contrast, the change in the Marine vapor source contribution depends on its signal downtown Cairo city and its lag-time controlled by the wind speed and distance of the concerned location from the Mediterranean coast. The aerodynamics prevailing between Cairo and the Mediterranean coast will always result in the shown different shifts in the signal arrival of the three vapor sources to the capital, according to the corresponding time-lag for each (12 hours for the Marine contribution, but zero hours for the ET and Sahara contributions). The vertical grey stripes in the top and bottom diagrams show the nighttime hours each day.

ALARM

Fig. 7 has two vertical axes. The reader must keep an eye on plot #11 in Figs 6 to get an idea about the relationship between the Marine vapor source mass contribution, WP, and the isotopic ratio of the AVM. The primary vertical axis in Fig. 7 reports the relationship between $d^{18}O$ of the AVM and time (large grey squares) while the secondary vertical axis is in use to communicate the relationship between the percent contributions of the three vapor sources and time on the x-axis. Accordingly, please do not refer to the Marine data-points in Fig. 7 and wrongly look for elusive projections for them on the primary vertical axis in this diagram. Otherwise, the wrong projection will lead to the false impression that the Marine vapor source data-points show up enriched isotopic compositions. Visibly, this alarm-statement also applies to the ET vapor source data-points.

Conclusions

Our method of hourly collecting artificial condensates in Summer proved successful to replace lacking CRDS device for isotopic measurement in atmospheric vapor mixture, AVM. For artificial Summer condensates with winter rain samples, data processing has given a quantitative distribution for each AVM into three end members using three new models, including temporal AVM $d^{18}O$ waveform with diurnal peak and nocturnal tunnel.

The moderate contribution of the ET vapor source stands behind the diurnal and hibernal enrichment in ACM ^{18}O. In contrast, the little input from the Troposphere source and the dominant Marine vapor input stand behind the nocturnal and estival AVM ^{18}O depletion. Diurnal convection and nocturnal advection, in the two seasons, resulted in a high-dispersion negative relationship between the mass contribution and $d^{18}O$ for the Marine vapor source, with low input by daytime and high input by nighttime. On the contrary, the ET source diurnal transmission shows a low-dispersion positive regression for such a relationship since ET has an increasing diurnal release. A 12-hour time-lag for the Marine source waveform results from the mingling of the turbulent and steady Marine vapor inputs by daytime and nighttime, respectively, via chaotic and calm air-masses and the lengthy trajectory from the Mediterranean coast to Cairo. In contrast, a Zero-hour time-lag is to observe for the other two vapor sources, due to shorter pathways under the same wind direction and speed, and the daytime-only-ET-vapor-release vs. the all-day Troposphere layer downdraft.

The used procedures give useful isotope and humidity information to improve understanding the water budget. The models help to run the evaporation experiments better. Interactive diagrams, for the relationship between percent input and AVM $d^{18}O$, explain the enriched ^{18}O signals of upstream Nile water as being a result of robust ET recycling at the head reaches. Recycling of Marine and ET vapor is to confirm for freshwater generation from the AVMs to fight drought, especially in Summer, at the mid-latitudes. Besides, the used models are successful in enhancing CRDS isotope measurements. These models are a breakthrough in isotope hydrology.

References

Abo el Fetouh, Y El-Askary, H El Raey, M Allali, M Sprigg, and W Kafatos, 2013. Annual Patterns of Atmospheric Pollutions and Episodes over Cairo, Egypt. Advances in Meteorology. 10.1155/2013/984853.

Benettin, P, Volkmann Till H. M., Freyberg Jana von, Frentress Jay, Penna Daniele, Dawson Todd E., and Kirchner James W. 2018. Effects of climatic seasonality on the isotopic composition of evaporating soil waters. Hydrol. Earth Syst. Sci., 22, 2881–2890.

Bonne, J., Behrens, M., Meyer, H. et al. Resolving the controls of water vapour isotopes in the Atlantic sector. Nat Commun 10, 1632, 2019. https://doi.org/10.1038/s41467-019-09242-6.

Chun-Ta, Lai, James R., Ehleringer J. R., Bond B. J., and Paw K. T. U., 2006. Contributions of evaporation, isotopic non-steady state transpiration and atmospheric mixing on the δ18O of water vapour in Pacific Northwest coniferous forests.

Plant, Cell and Environment, 29, 77–94.

Cox, K. A., Rohling, E. J., Schmidt, G. A., Schiebel, R., Bacon, S., Winter, D. A., Bolshaw, M., and Spero, H. J.: New constraints on the Eastern Mediterranean δ18O:δD relationship, Ocean Sci. Discuss., 8, 39–53, https://doi.org/10.5194/osd-8-39-2011, 2011. This discussion paper was not published.

Evan, A T, C Flsmsnt, C Lavaysse, C Kocha, and A Saci. 2015. Water Vapor–Forced Greenhouse Warming over the Sahara Desert and the Recent Recovery from the Sahelian Drought. J. of Climate, 28, 108-123.

Fiorella R, West J B, and Bowen G J. 2019. Biased estimates of the isotope ratios of steady-state evaporation from the assumption of equilibrium between vapour and precipitation. Hydrological Processes. 2019; 33:2576–2590.

Flaux C, Claude C, Marriner N, and C Morhange, 2013. A 7500-year strontium isotope record from the northwestern Nile delta (Maryut lagoon, Egypt). Quaternary Science Reviews 78 (2013) 22e33. http://dx.doi.org/10.1016/j.quascirev.2013.06.018

Follstad Shah J.J, Y Jameel, R M Smith, RS Gabor, P D Brooks, and SR Weintraub, 2019. Spatiotemporal Variability in Water Sources Controls Chemical and Physical Properties of a Semi-arid Urban River System. Journal of the American Water Res. Assoc. 1–17. https://doi.org/10.1111/1752-1688.12734.

Frankenberg, C, Yoshimura K, Warneke T, Aben I, Butz A, Deutscher N, Griffith D, Hase F, Notholt J, Schneider M, Schrijver H and Röckmann,.2009. Dynamic processes governing lower-tropospheric HDO/H2O ratios as observed from space and ground, Science, 325(5946), 1374–1377

Galewsky J, C Rella, Z Sharp, K Samuels, and D Ward, 2011. Surface measurements of upper tropospheric water vapor isotopic composition on the Chajnantor Plateau, Chile, Geophys. Res. Lett., 38, L17803, DOI:10.1029/2011GL048557.

Galewsky, J., H C Steen-Larsen, R D Field, J Worden, C Risi, and M Schneider, 2016. Stable isotopes in atmospheric water vapor and applications to the hydrologic cycle, Rev. Geophys.,54, 809–865, DOI:10.1002/2015RG000512.

Gasse, F., 2000. Hydrological changes in the African tropics since the Last Glacial Maximum. Quaternary Science Reviews 19, 189-211.

Guilpart, E., F Vimeux, S Evan, J Brioude, J-M Metzger, C Barthe, C Risi, and O Cattani, 2017. The isotopic composition of near-surface water vapor at the Maïdo observatory (Reunion Island, southwestern Indian Ocean) documents the controls of the humidity of the subtropical troposphere, J. Geophys. Res. Atmos.,122, 9628–9650, DOI:10.1002/2017JD026791.

Helliker B R, Roden J R, Cook C, and J R Ehleringer, 2002. A rapid and precise method for sampling and determining the oxygen isotope ratio of atmospheric water vapor. Rapid Commun Mass Spectrom 16:929–932. https://onlinelibrary.wiley.com/doi/epdf/10.1002/rcm.659

Helliker B R and D Noone, 2010. Novel Approaches for Monitoring of Water Vapor Isotope Ratios: Plants, Lasers, and Satellites DOI: 10.1007/978-90-481-3354-3_4. Chapter 4, p 71-88, in Isoscapes: Understanding movement, pattern, and process on Earth through isotope mapping. Jason B. West · Gabriel J. Bowen Todd E. Dawson · Kevin P. Tu (Editors). DOI 10.1007/978-90-481-3354-3. Springer.

Hussein A, 2018. Water balance of the Aswan High Dam Reservoir, Faculty of Mathematics and Natural Sciences, Institute for Natural Resource Conservation, Kiel University, Germany, 24118, Kiel, Deutschland, 65 p.

Lai X, J S Wright, W Huang, J Liang, G Lin, and S Zhu, 2018. Contributions of Atmospheric Transport and Rain–Vapor Exchange to Near-Surface Water Vapor in the Zhanjiang Mangrove Reserve, Southern China: An Isotopic Perspective. Atmosphere, 9, 365. DOI:10.3390/atmos9090365.

Kalabokas P D, J-P Cammas, V Thouret, A Volz-Thomas D Boulanger, and CC Repapis, 2013. Examination of the atmospheric conditions associated with high and low summer ozone levels in the lower troposphere over the eastern Mediterranean, Atmos. Chem. Phys., 13, 10339–10352, 2013. DOI:10.5194/acp-13-10339-2013

Khozyem, H., 2020.

An Overview of Paleo-Climate Evidence in Egypt. In Omran E.-S. E. and A.M. Negm (eds.), *Climate Change Impacts on Agriculture and Food Security in Egypt*, Springer Water, https://doi.org/10.1007/978-3-030-41629-4_2

Marchina C, Natalie C, and G Bianchini, 2019. The Po River Water Isotopes during the Drought Condition of the Year 2017. Water, 11, 150. DOI:10.3390/w11010150.

Mercer JJ, Liefert D T, and Williams D G. 2020. Atmospheric vapor and precipitation are not in isotopic equilibrium in a continental mountain environment. Confidential manuscript submitted to Hydrological Processes.

Neef, A. Tropical forests lost to land grabbing. Nat. Geosci. 13, 460–461 (2020). https://doi.org/10.1038/s41561-020-0604-3.

https://www.nature.com/articles/s41561-020-0604-3?utm_source=ngeo_etoc&utm_medium=email&utm_campaign=toc_41561_13_7&utm_content=20200703&sap-outbound-id=153369A44CB53BA9FA8FA2080EA15B4A24017BED

Noone D, J Galewsky, Z D Sharp, J Worden, J Barnes, D Baer, A Bailey, D P Brown, L Christensen, E Crosson, F Dong, J V Hurley, L R Johnson, M Strong, D Toohey, A V Pelt and J S Wright, 2011. Properties of air mass mixing and humidity in the subtropics from measurements of the D/H isotope ratio of water vapor at the Mauna Loa Observatory. J. Geophys. Res. Atmos, 116, 898–908.

Noone D, 2011. Pairing Measurements of the Water Vapor Isotope Ratio with Humidity to Deduce Atmospheric Moistening and Dehydration in the Tropical Mid troposphere. J. Climate, vol. 25, 4476-4494. https://doi.org/10.1175/JCLI-D-11-00582.1

Penchenat T, Vimeux F, Daux V, Cattani O, Viale M, Villalba R, Srur A, and Outrequin C. 2020. Isotopic equilibrium between precipitation and water vapor in Northern Patagonia and its consequences on $d^{18}O_{cellulose}$ estimate. Am. Geophysical Union, doi: 10.1029/2019JG005418

Peng, T-R, Chun-Chun Huang, C-C, & Jui-Er Chen, J-E, Zhan, W-J, Chiang, L-W, and L-C Chang, 2016.
Evaluating the Relative Importance of Groundwater Recharge Sources in a Subtropical Alluvial Plain Using Tracer-Based Ternary End Member Mixing Analysis (EMMA).
Water Resour Manage (2016) 30:3861–3878
DOI 10.1007/s11269-016-1393-8

Peng, T-R, Zhan, W-J, Tong, L-T, Chen, C-T, Liu, T-S, and W-C Lu, 2018.
Assessing the recharge process and importance of montane water to adjacent tectonic valley-plain groundwater using a ternary end-member mixing analysis based on isotopic and chemical tracers.
Hydrogeology Journal. https://doi.org/10.1007/s10040-018-1741-2

Risi C, S Bony, F Vimeux, C Frankenberg. D Noone and J Worden, 2010. Understanding the Sahelian water budget through the isotopic composition of water vapor and precipitation. J. Geophys. Res. Atmos, 115, D24.

Risi, C, C Muller and Blossey P, 2020
What controls the water vapor isotopic composition near the surface of tropical oceans? Results from an analytical model constrained by large-eddy simulations. American Geophysical Union.
https://doi.org/10.1029/2020MS002106

Skrzypek G, A Mydłowski, S Dogramaci, P Hedley, JJ Gibson, and P F Grierson, 2015. Estimation of evaporative loss based on the stable isotope composition of water using Hydrocalculator. J. Hydrol, 523, 781-789.

https://www.sciencedirect.com/science/article/pii/S0022169415001134?via%3Dihub

Stephens GL, Slingo JM, Rignot E, Reager JT, Hakuba MZ, Durack PJ, Worden J, Rocca R. 2020. Earth's water reservoirs in a changing climate. Proc. R. Soc. A. 476: 20190458. http://dx.doi.org/10.1098/rspa.2019.0458

Thambiran Tirusha_2006. Vertical distribution of tropospheric ozone over Cairo, Egypt. M. Sc. Thesis, University of KwaZulu-Natal, South Africa, 162 p.

Viviroli, D., Kummu, M., Meybeck, M. *et al.* Increasing dependence of lowland populations on mountain water resources. *Nat Sustain* (2020). https://doi.org/10.1038/s41893-020-0559-9

Zhao L, L. Wang, X. Liu, H. Xiao, Y. Ruan, and M. Zhou, 2014.
The patterns and implications of diurnal variations in the d-excess of plant water, shallow soil water, and air moisture. Hydrol. Earth Syst. Sci., 18, 4129–4151, 2014. doi:10.5194/hess-18-4129-2014

Zhao L, Liu X, Wang N, Kong Y, Song Y, He Z, Liu Q, and L Wang, 2019.
Contribution of recycled moisture to local precipitation in the inland Heihe River Basin. Agriculture and Forest Meteorology, vol 271, 15, 316-335.

https://www.sciencedirect.com/science/article/pii/S0168192319301261?fbclid=IwAR0twtNgmMfuUMk8lkHvixSn4d6chcqrs7WS1UTeAj6QSxMYz7xj6Oq0nDk

Zhang, J., Genty, D., Sirieix, C., Michel, S., Minster, B., Régnier, E., 2020. Quantitative assessment of moisture source and temperature governing rainfall δ18O from 20 years-long monitoring records in SW-France: Importance for isotopic-based climate reconstructions, Jour Hydrol,
https://doi.org/10.1016/j.jhydrol.2020.125327

1. http://worldpopulationreview.com/countries/egypt-population/
2. https://relay.nationalgeographic.com/proxy/distribution/public/amp/science/2018/09/news-meghalayan-holocene-megadrought-archaeology?__twitter_impression=true&fbclid=IwAR3gW8HDN6WUCNwXW_uW69mwvIMT1Te9qTb2XtfsChyVhVPSx13i710z9Q4
3. https://www.facebook.com/GeomorphologyRules/posts/2219848234739092
4. https://www.sciencedirect.com/science/article/pii/S2090123210001098
5. https://www.sciencedirect.com/science/article/pii/S2090447913000117
6. https://www.geolounge.com/deforestation-is-drying-up-atmospheric-rivers/?fbclid=IwAR3LoeeeF52GhRRRmXArrwppNuJxfh1xmQvoYnmi7IO1RbGyud3zcMWypZw

Declarations

Conflict of interest

We have no conflict of interest to declare.

Tables

Due to technical limitations, tables 1-2 are only available as a download in the supplemental files section.

Figures

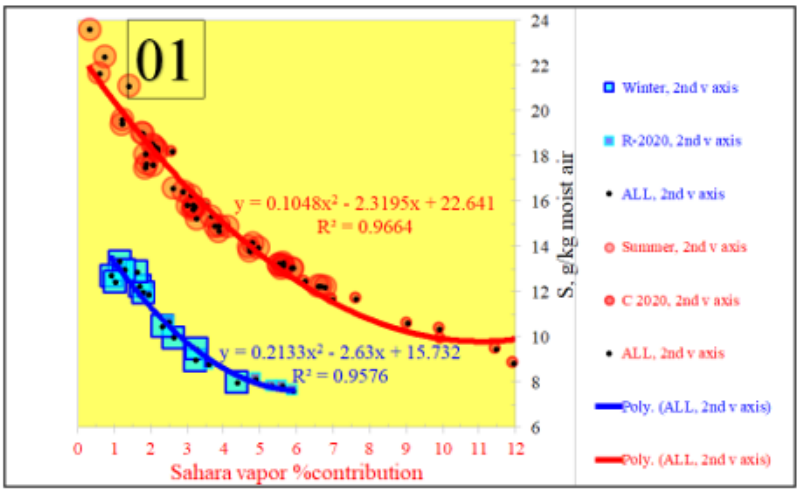

Figure 1

Negative curvilinear relationships between S (on the y-axis) and Tropospheric vapor % input (on the y-axis). Tropospheric vapor % input values appear at higher S levels in Summer.

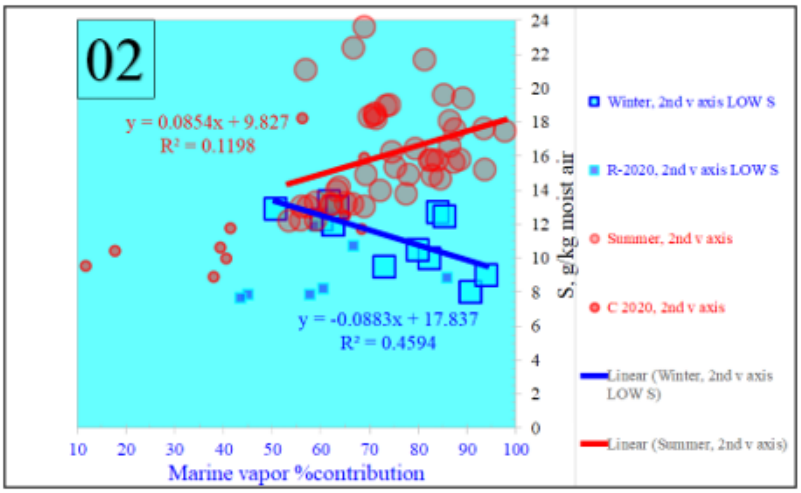

Figure 2

Relationships between S (on the y-axis) and Marine % input (on the y-axis). The estival input has positive regression, contrary to a negative regression in Winter.

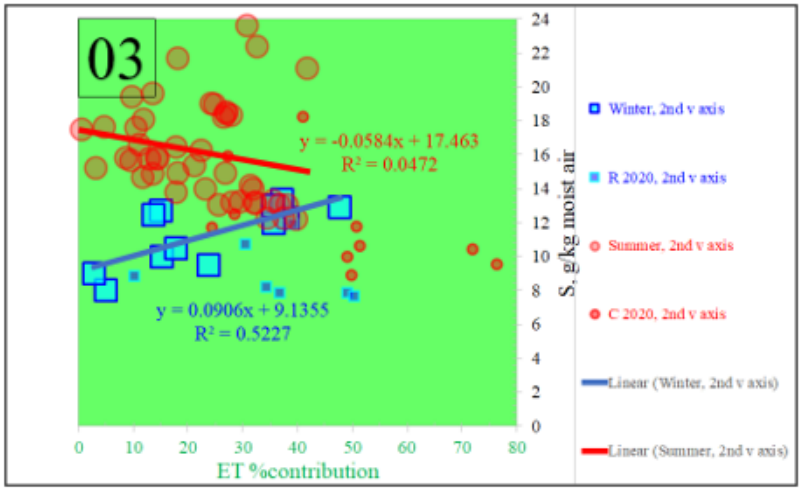

Figure 3

Relationship between S (on the y-axis) and ET % input (on the x-axis), with a positive regression in Winter.

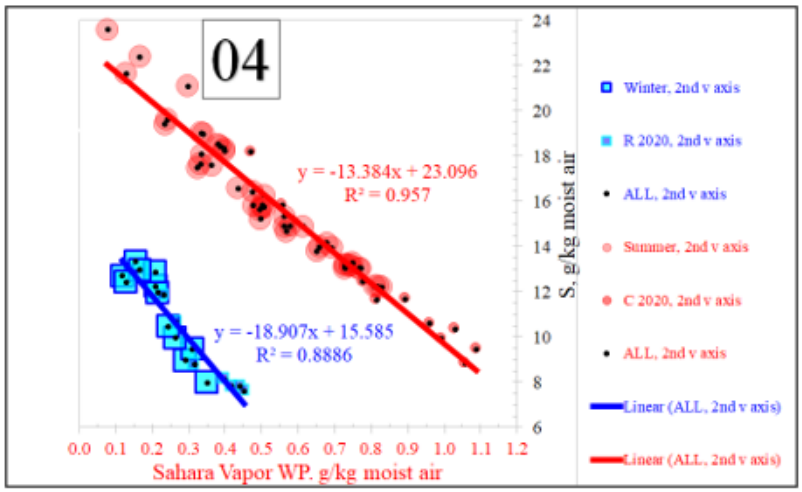

Figure 4

A negative linear relationship between S (on the y-axis) and Tropospheric WP (on the y-axis).

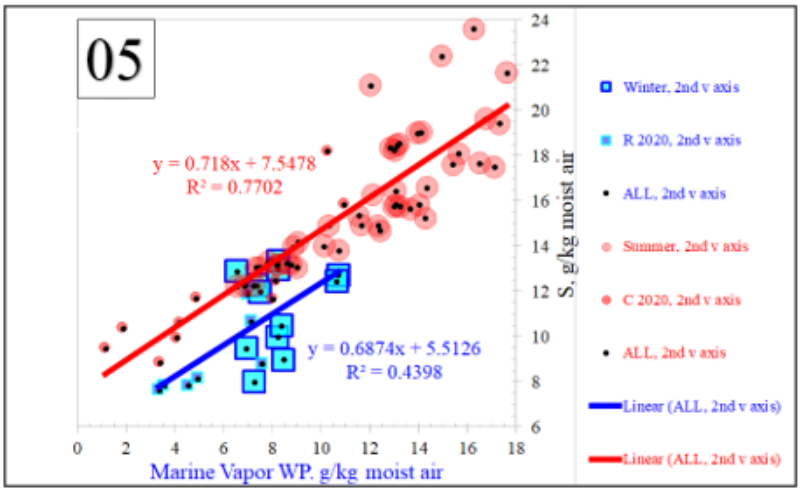

Figure 5

A significant positive linear relationship between S values (on the y-axis) and Marine WP (on the x-axis) for the two seasons, with a higher intercept in Summer. The Marine WP values have a broader range in Summer than in Winter.

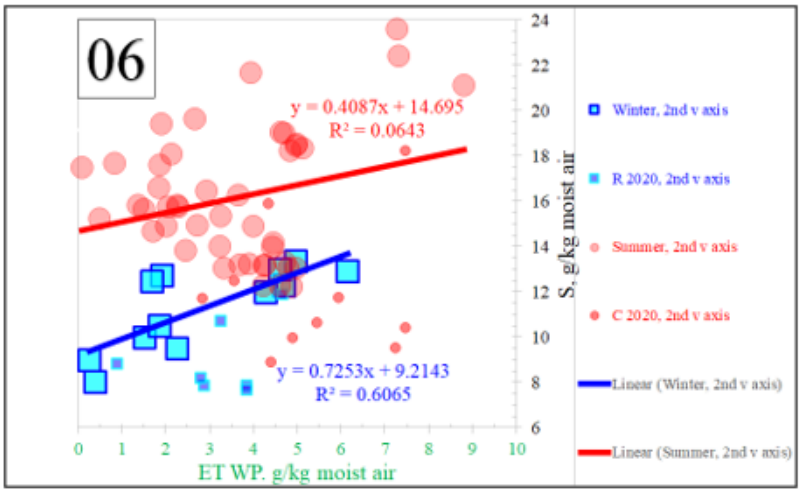

Figure 6

Relationship between S (on the y-axis) and ET WP (on the x-axis). Higher intercept in Summer than in Winter.

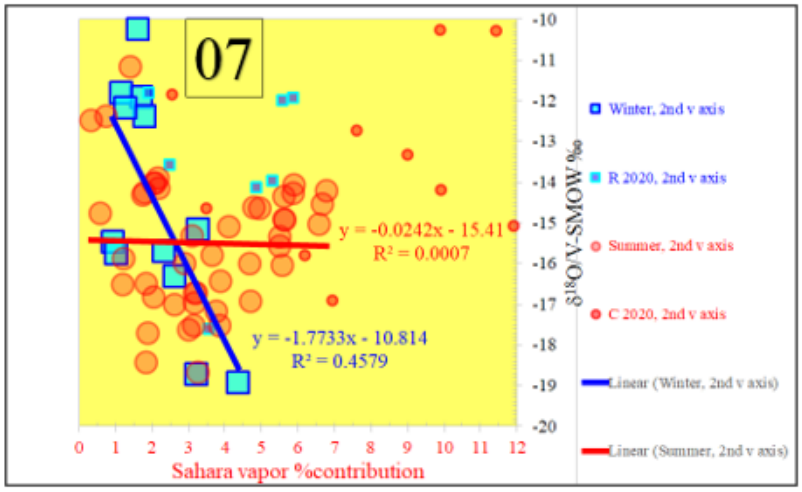

Figure 7

Random relationship between δ18O (on the y-axis) and Tropospheric % input (on the x-axis).

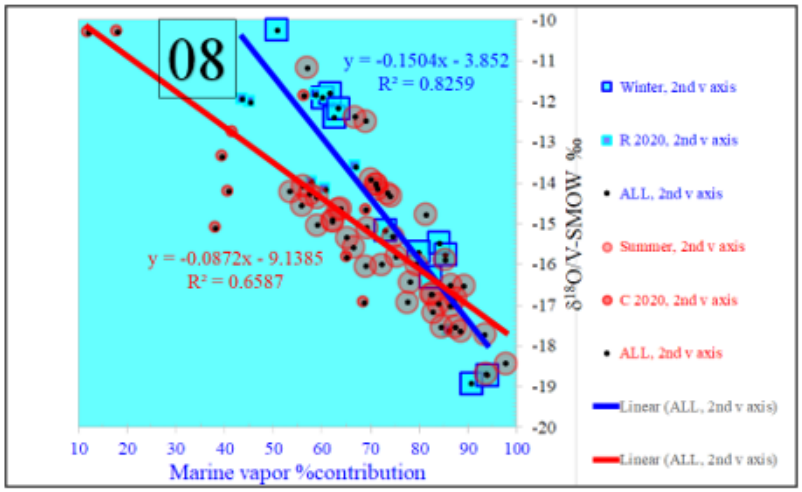

Figure 8

Significant negative linear relationship between δ18O (on the y-axis) and Marine % input (on the x-axis).

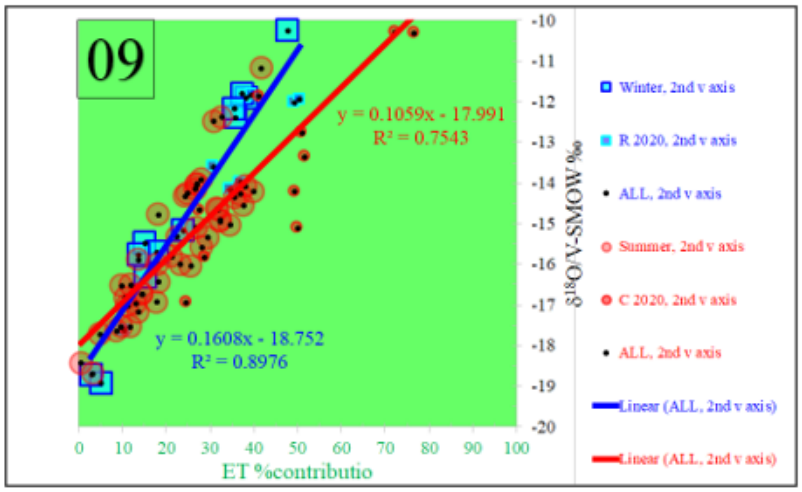

Figure 9

The significant positive relationship of δ18O (on the y-axis) with ET % input (on the y-axis).

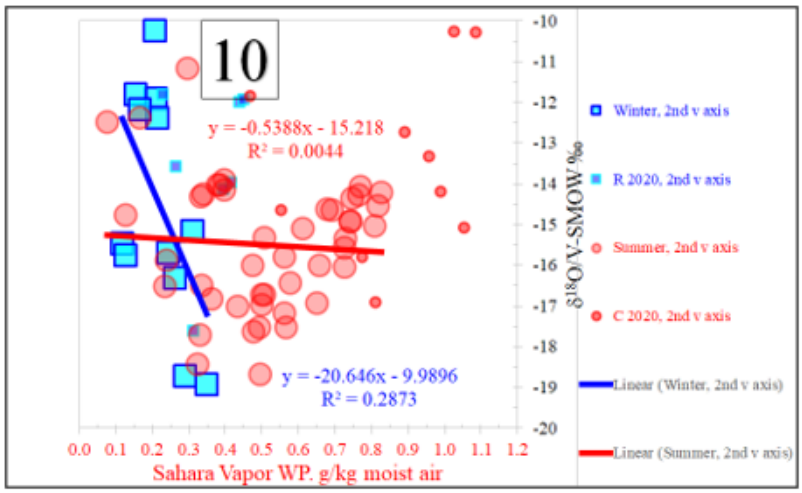

Figure 10

The random relationship between δ18O (on the y-axis) with Tropospheric WP (on the y-axis).

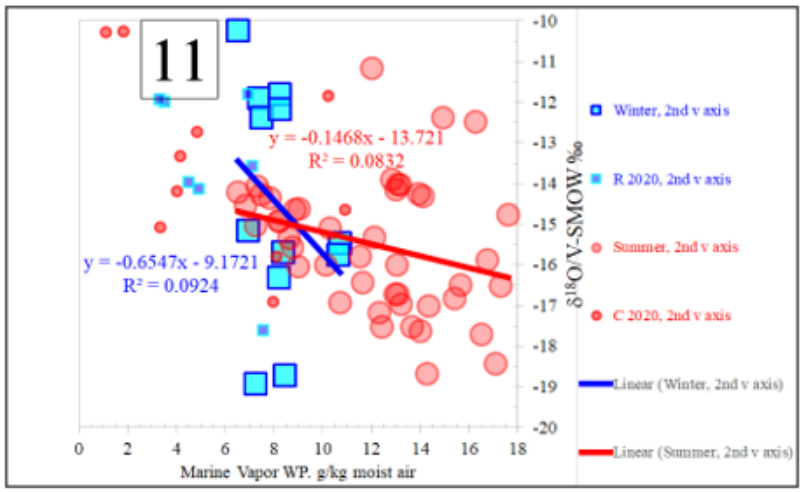

Figure 11

Random relationship between δ18O (on the y-axis) and the Marine WP (on the y-axis), same as in Fig 20.

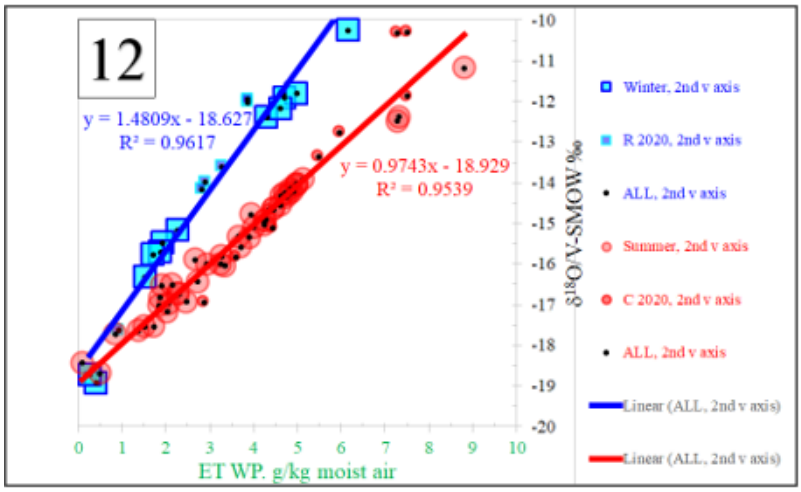

Figure 12

The significant positive linear relationship between δ18O (on the y-axis) and the ET WP (on the y-axis).

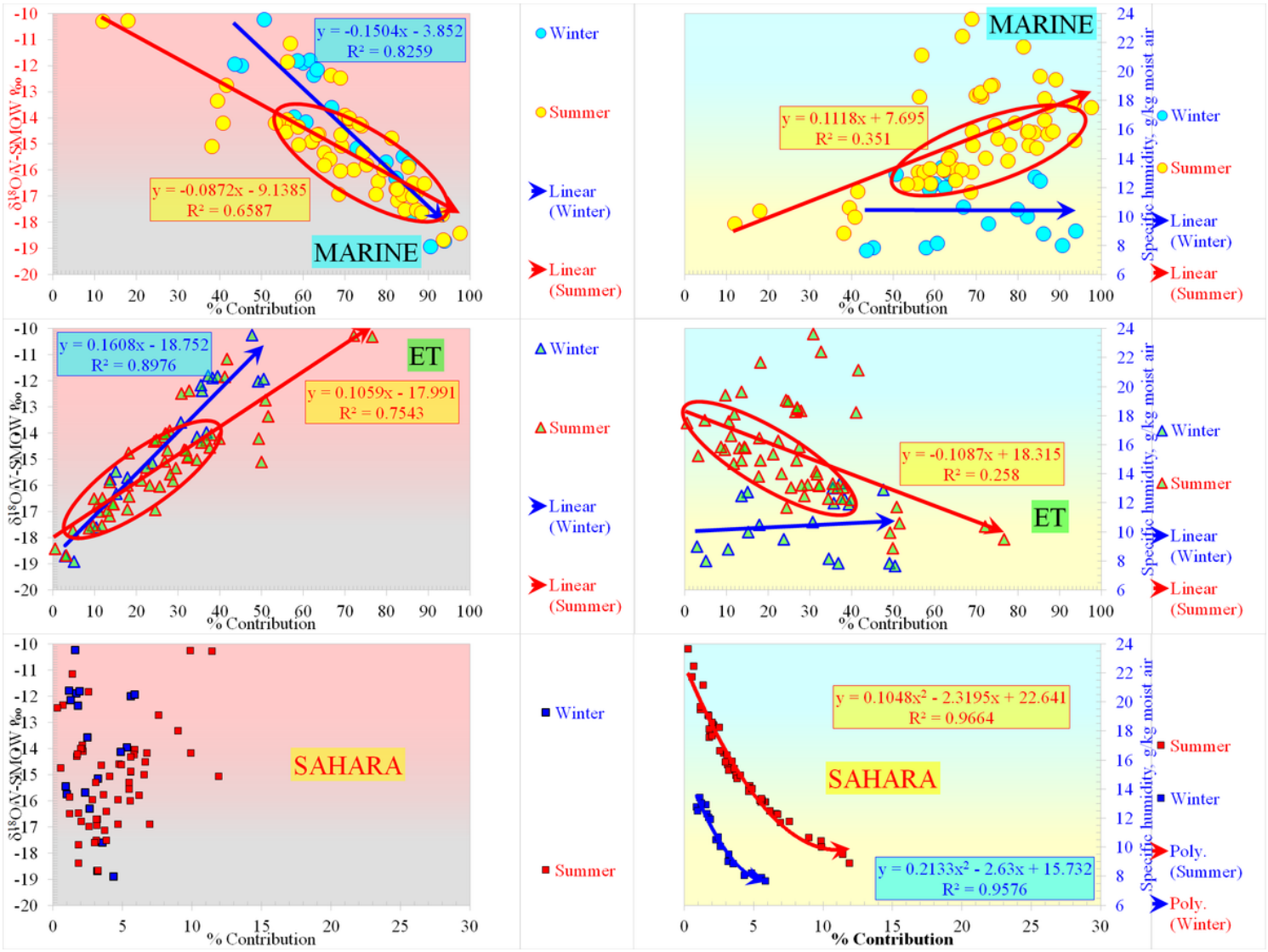

Figure 13

The relationship between the isotopic composition and the percent contribution (left-hand side diagrams) and the relationship of the S values with the percent contribution (right-hand side diagrams) for the three vapor sources making the local atmospheric vapor mixtures. The information provided by the two types of plots is complementary.

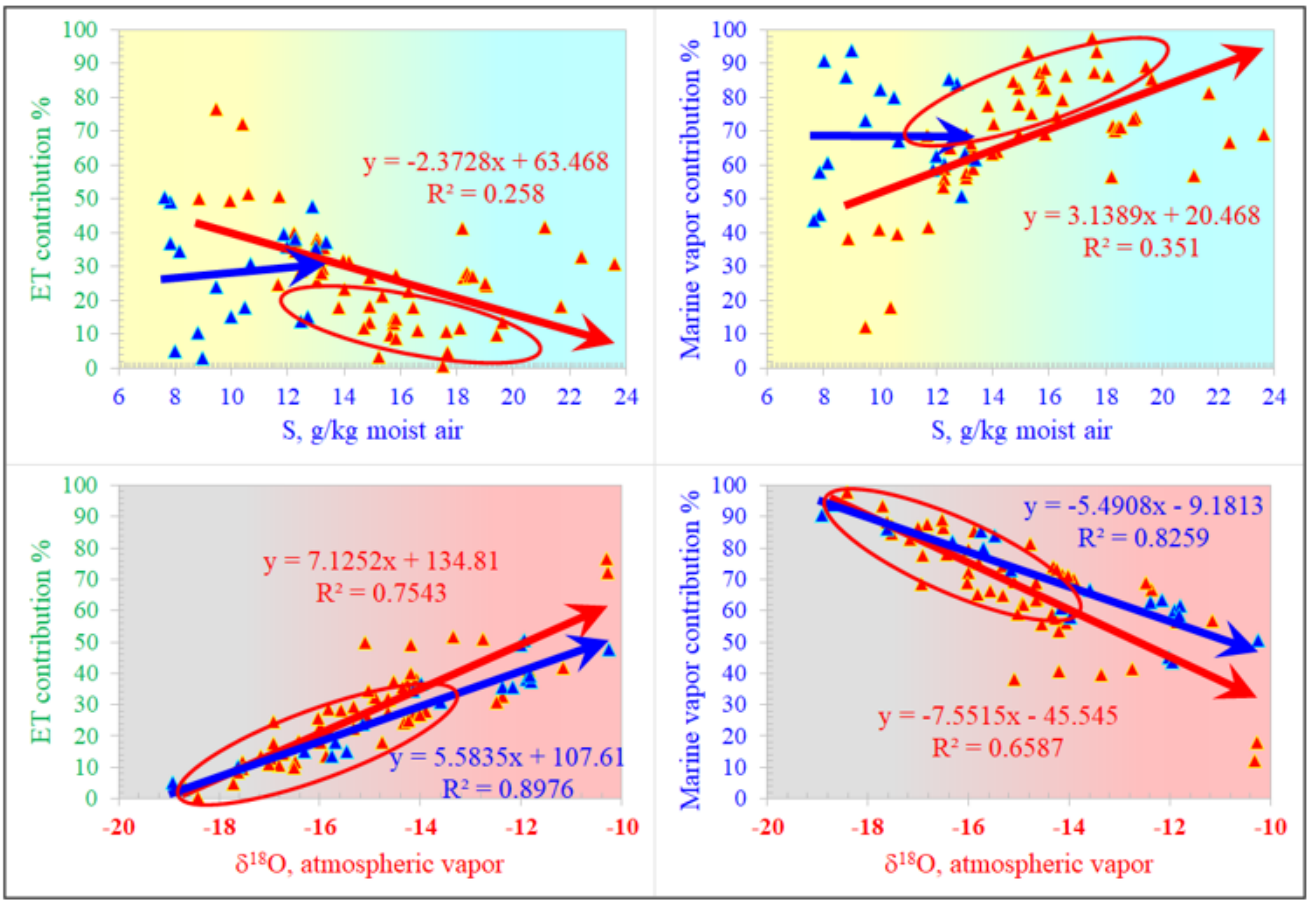

Figure 14

Comparison of the percent contribution to the S value relationship (top diagrams) and the percent contribution to δ18O values relationship (bottom diagrams) for the ET vapor source (left-hand side diagrams) and the Marine vapor source (right-hand side diagrams). The information provided by the four plots is visibly showing the opposite trends of these two vapor sources. The higher ET contribution goes with, the lower S values and the enriched signatures of the atmospheric vapor mixtures while the high Marine vapor contribution goes with the higher S values and the depleted signals of the atmospheric vapor mixtures. The locus of Winter data-points appear above (in the left-hand side diagrams) or below (in the right-hand side diagrams) the locus of Summer data-points in harmony with the opposite behaviors of the two vapor sources. The contribution of the ET source (not its isotopic composition) is the primary controller of the isotopic depletion of the atmospheric vapor mixtures (bottom left corner diagram). Besides, the potential supremacy of the mass action of the evaporation component over transpiration in the Nile Delta lands in Summertime will not significantly change the isotopic composition of the combined ET term. This analysis is to understand by observing that the irrigation water is isotopically more enriched by evaporation in Winter compared to the case in Summer (due to the minimum discharge from Lake Nasser reservoir in Winter via the partial closure of the irrigation canals downstream) vs. the high discharge from the Lake in the hot season. Also, the low Winter temperatures will lead to making the isotopic composition of the vapor released by the evaporation of soil water in Winter, almost like that for the vapor released by soil water evaporation in Summer (since the fractionation factor is higher under the low temperature).

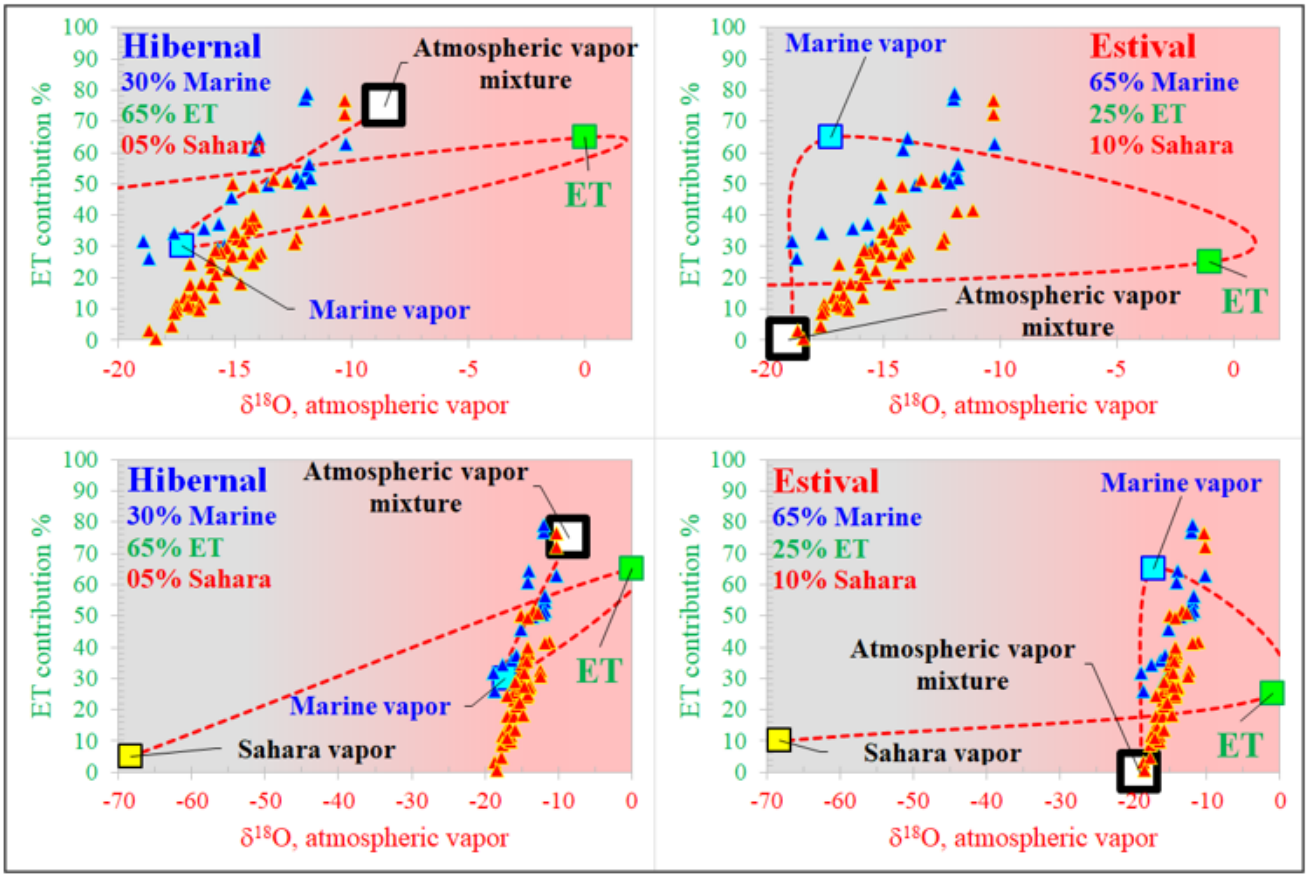

Figure 15

Interactive diagrams based on the left bottom corner diagram shown in Fig 14.

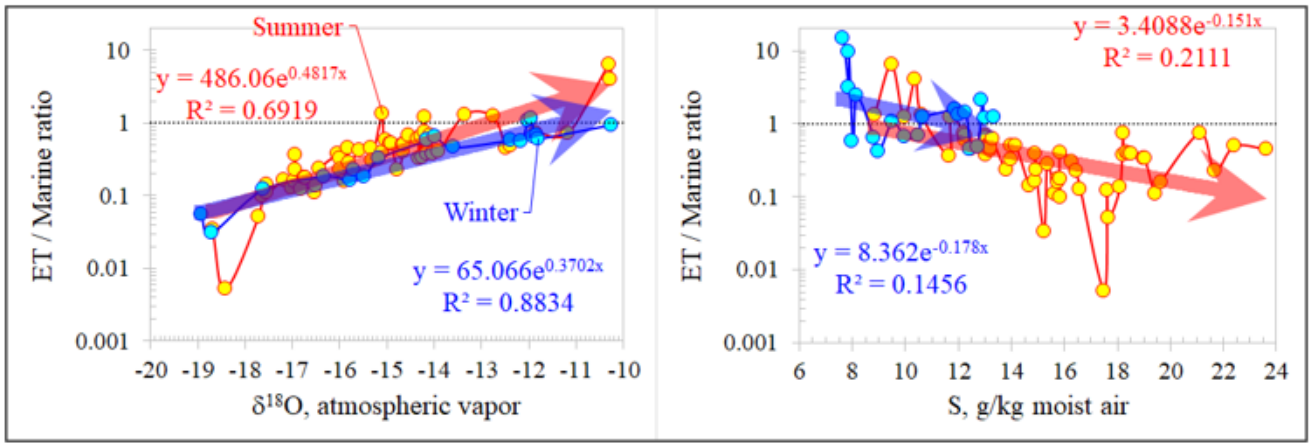

Figure 16

The relationship of the ET to Marine moisture contribution ratio with the isotopic composition (left-hand side diagram) and S value (right-hand side) of the local atmospheric vapor mixtures in Winter and Summer

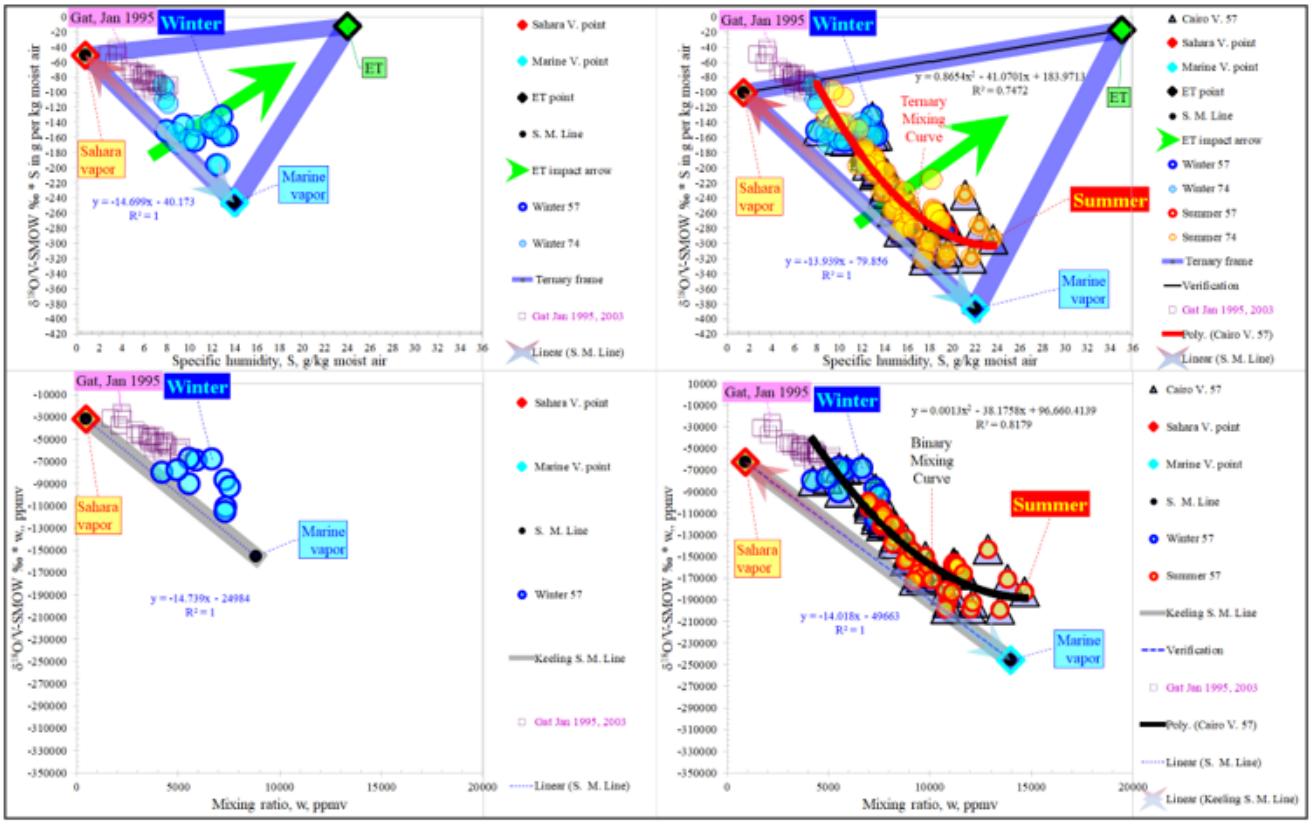

Figure 17

Four "Korean-style" diagrams for the relationship of the humidity (S or w) on the x-axis with the product of the isotopic ratio and S (or w) on the y-axis. The top diagrams show the Ternary Mixing case with S on the x-axis, while the bottom diagrams show the Binary Mixing model with w on the x-axis. The left-hand side diagrams show Winter exhalation (humidity shrinkage for the local AVMs and their vapor sources to a minimum) whereas the right-hand side diagrams show Summer inhalation (humidity expansion for the local AVMs and their vapor sources to a maximum). In the top charts, the impact of the isotopically enriched ET moisture source is visible in dragging the data-points to the upper right-hand side corner.

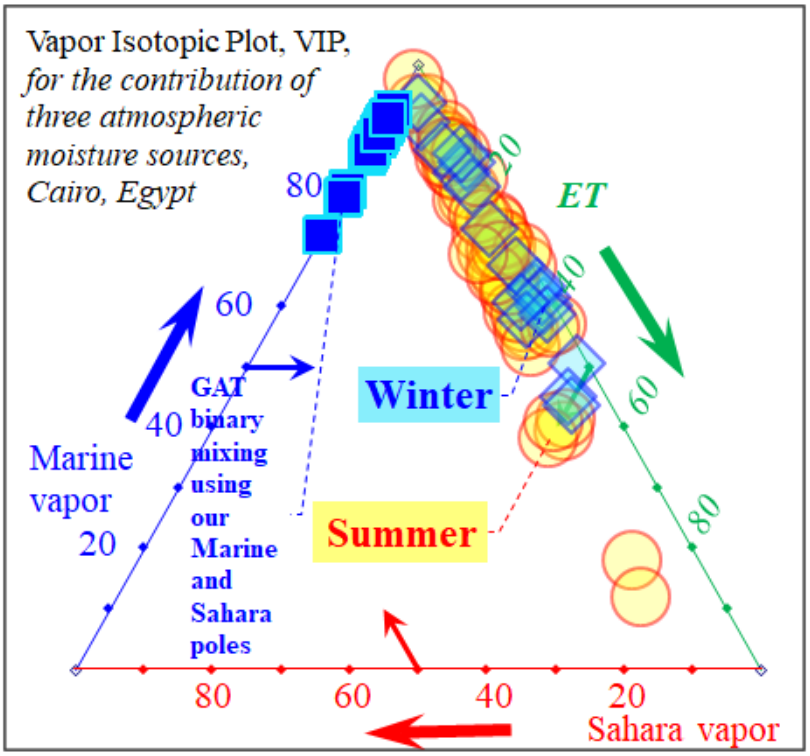

Figure 18

Piper diagram for the three components that make the local atmospheric vapor mixtures downtown Cairo. The Gat data-points of Jan 1995. shown at the upper left-hand side corner, are based on the binary mixture of the two vapor sources, namely the Marine and the Tropospheric sources since we do not know the isotopic composition and S value for the potential ET term in Gat vapor samples

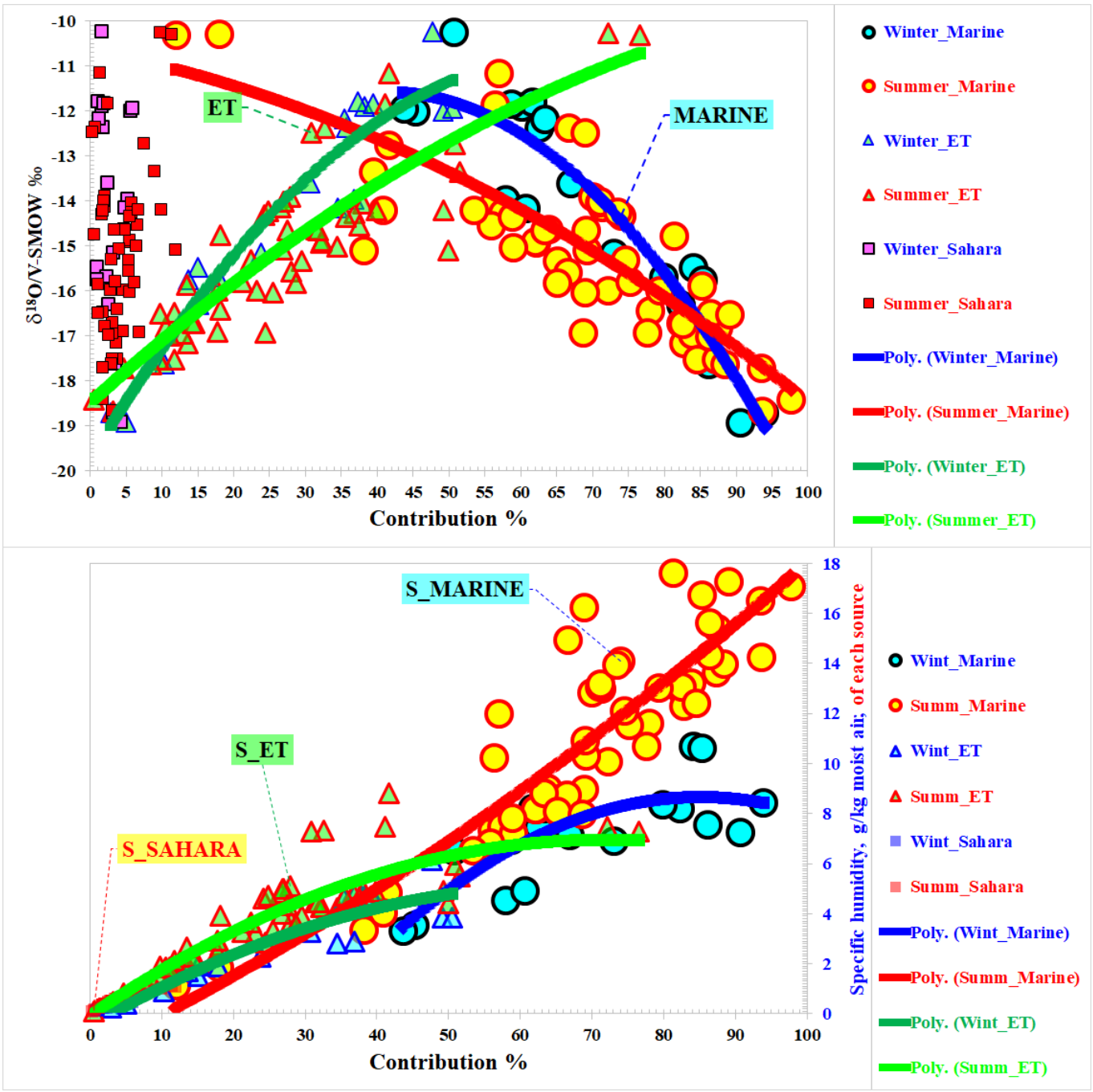

Figure 19

The distinct distributions of the three vapor sources in Winter and Summertime are to observe in the top diagrams of the relationship of the isotopic composition and the percent contribution, with the trend of the ET source be opposite to that of the Marine vapor source. The increase of the contribution of the Marine vapor source visibly leads to the isotopic depletion of the atmospheric vapor mixtures while the increase of the ET vapor source contribution leads to the isotopic enrichment of the atmospheric vapor mixtures. The bottom diagram is showing the superiority of the Marine vapor source, especially in Summertime, for the relationship of S values, on the y-axis, with the percent contribution of the three vapor sources, on the x-axis.

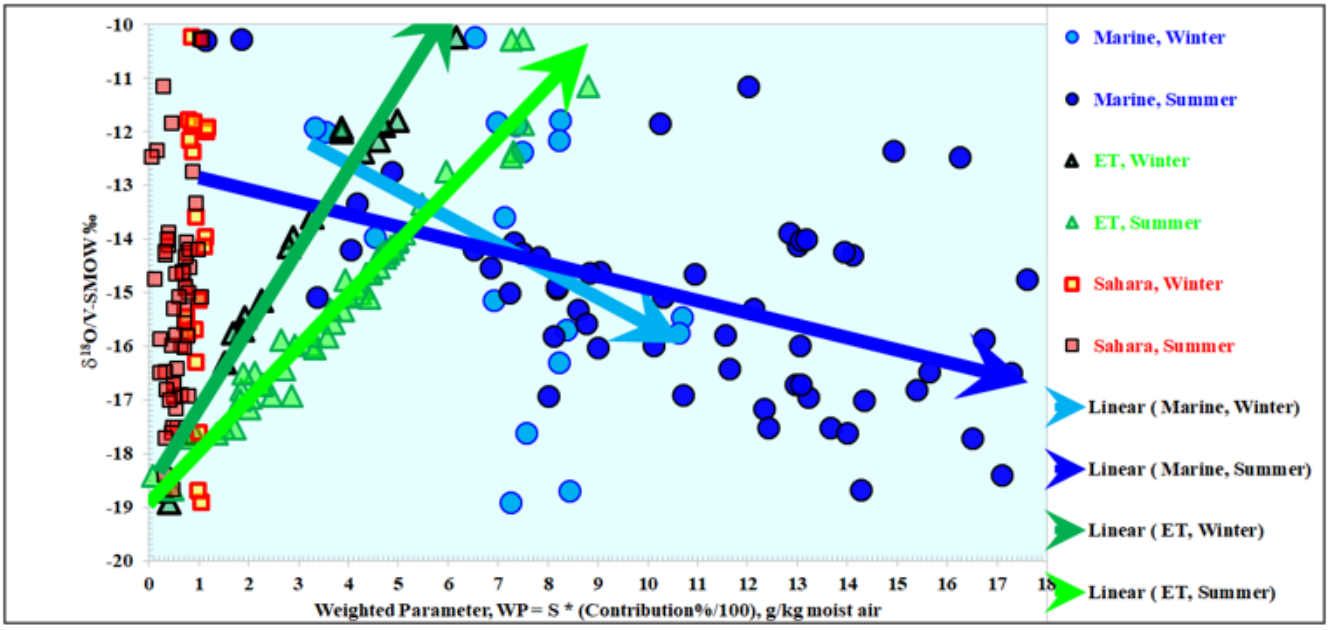

Figure 20

The TIMAM model relationship between the isotopic composition of the AVMs and the WP values of the three vapor sources. The dominance of the Marine vapor source is highly visible, especially in Summertime. The dominant vapor source is showing high dispersion. In contrast, the ET source has much less dispersion. The Sahara vapor source shows the lowest WP values (red squares to the left-hand side) that increase in Summertime. The increase of the Marine vapor source WP values is showing a negative trend with 18O values while the ET vapor source is positively related to the 18O values in the two seasons with a steeper slope for its Winter data-points. The Marine vapor regime is active day and night, while the ET regime has primarily a diurnal activity that stands behind its lower dispersion. The high dispersion in the Marine vapor source data-points is related to the wide gap between its high (nocturnal) and low (diurnal) contributions, its long trajectory (180 km) and as such, it needs 36-hours for its signal transmission to reach in Cairo (with a mean wind speed of 5 km/hour) while the ET data-points have a shorter trajectory (120 km) and needs 24-hours to reach the capital (with the same wind speed given above). Also, the transmission by diurnal speedy convection wind (for the ET signal) leads to much less ET data-point scattering while the blend mingling of diurnal (rapid convection) and the nocturnal (steady advection) transmissions by wind (for the Marine vapor signal) leads to much dispersion. The ET data-points with high WP values (pointing towards the right-hand-side of the plot) correspond to daytime while its data-points with low WP values correspond to nighttime. Also, the data-points with high 18O contents correspond to daytime, while the data-points with low 18O contents correspond to nighttime. The same configuration is to see in Fig 11. The higher contributions of the Marine vapor source correspond to nocturnal observations at Cairo, while higher contributions of the ET source correspond to diurnal observations, as seen on the secondary vertical axis of Fig. 24. However, in other locations between the Mediterranean coast and Cairo city, the high Marine vapor contribution would appear by daytime, Fig. 24, due to the time-lag phenomena for such a Maritime vapor.

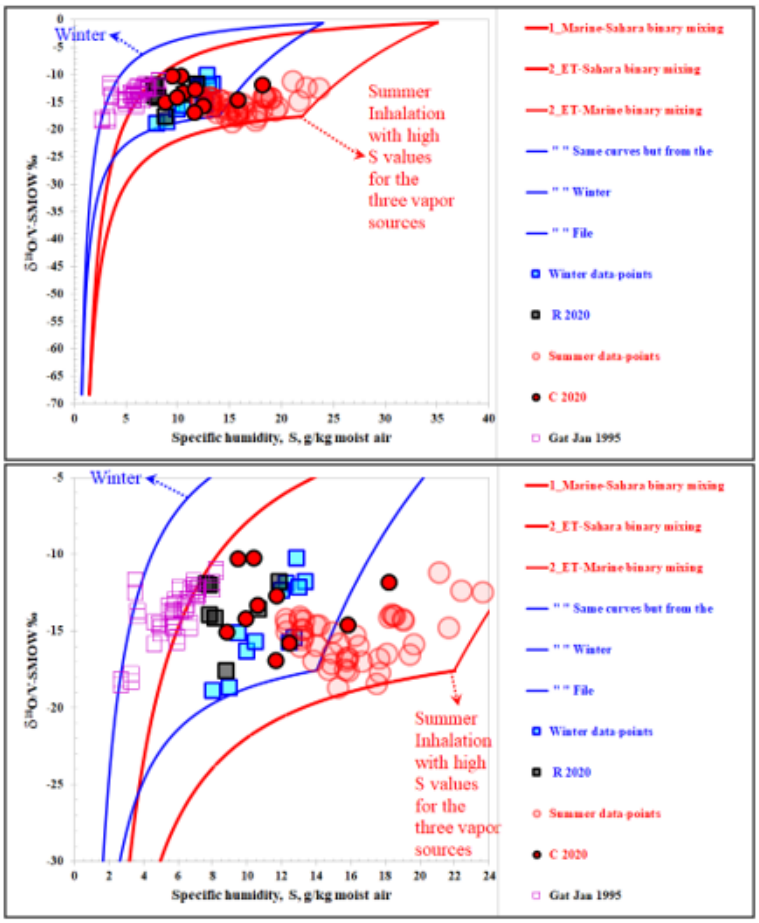

Figure 21

Curved wedge frameworks produced by CLAW model (blue curves for Winter, but red curves for Summertime) including our data-points for Winter (blue and black squares) and Summertime (red circles and red spots). The eastern Mediterranean basin data-points (Gat Jan 1995) are in purple void squares (to the left-hand side). They show up inside the Winter exhalation blue framework, but outside the Summer inhalation red framework. Sim S values in Cairo city in Summertime are higher than S values in the southern Amazon basin.

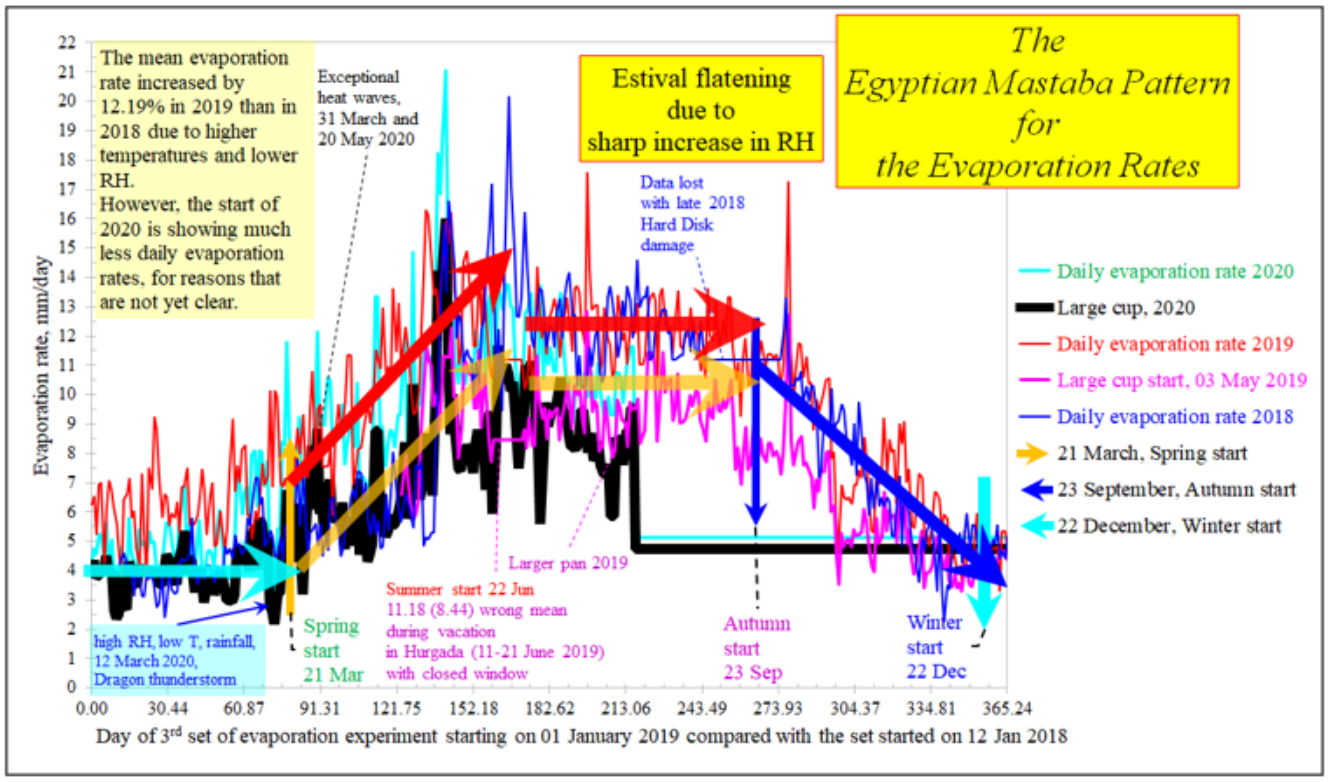

Figure 22

The daily evaporation rates, downtown Cairo city, for the years 2018, 2019, and 2020 (up to Friday, the 31st of July 2020). The evaporation rate increase in Spring is due to the dominance of low ambient humidity contents that persist up to the start of Summertime.

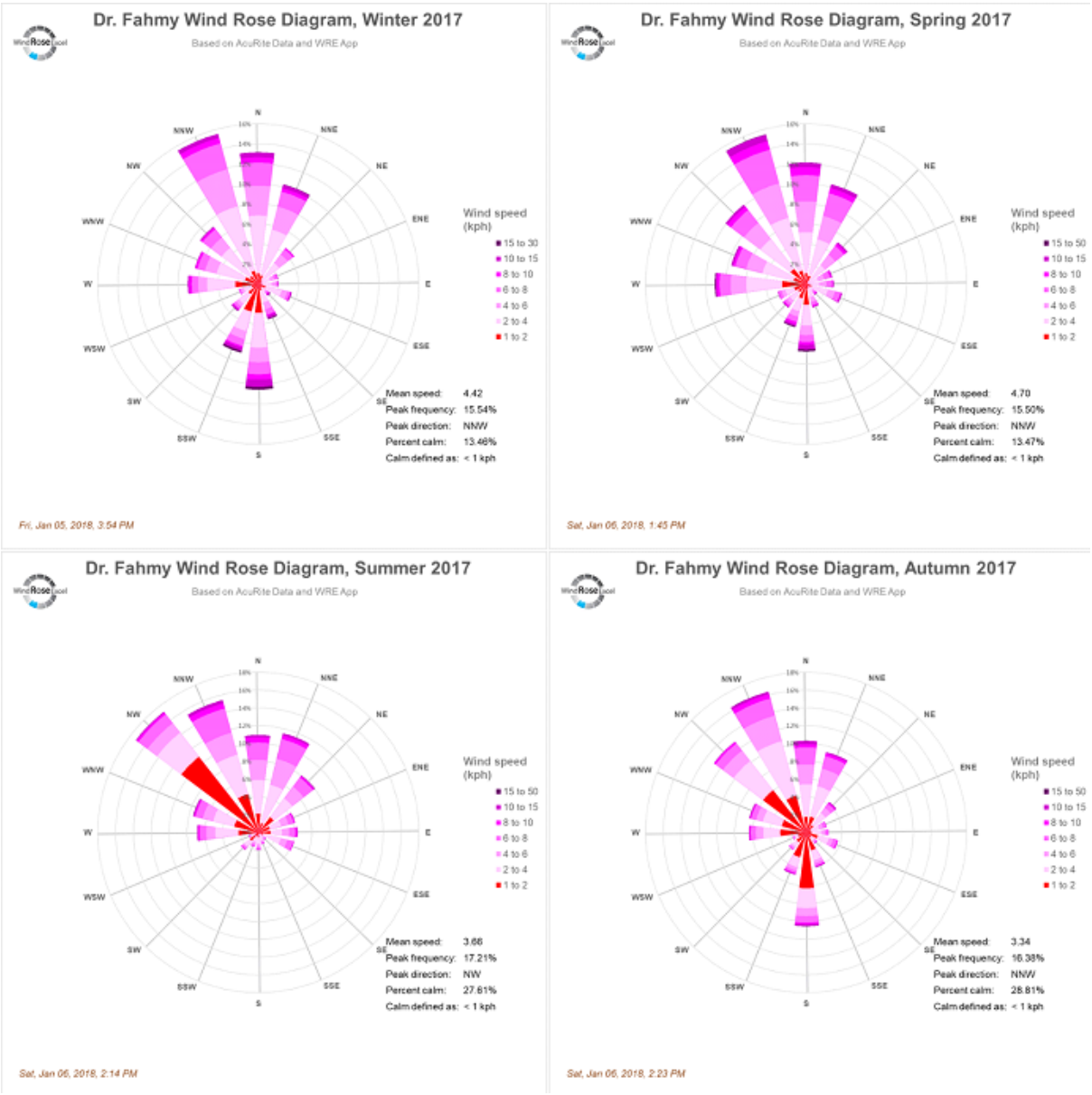

Figure 23

A wind rose diagram for downtown Cairo, Egypt, 2017. The Summer Marine northern wind (shown at the left bottom corner) blows inland and goes southward as far as reaching Cairo city, 180 km south of the Mediterranean Sea coast, after passing by the vast Nile Delta cultivated lands, where it gains additional humidity, to finally have about three times more S values, in the hot season, than the S values known for the northern Winter wind. Winter also has a southern wind component (as shown at the left top corner) blowing out from the Sahara, and goes farther northward to Cairo city, and partially resists the transmission of the Marine and ET signals to the capital especially in the cold season. We assume a mean northern wind speed of 5 km/hr. This speed will impose a 36-hr delay on the diurnal and nocturnal Marine isotopic and humidity signals to arrive at Cairo across 180 km (the distance between the Mediterranean coast and Cairo city). The ET vapor source has a 24-hr delay for its diurnal isotopic and humidity signals to cross a 120 km distance between a point in the middle of the northern sector of the Nile Delta (i.e., 60 km to the south of the Mediterranean coast) and Cairo city.

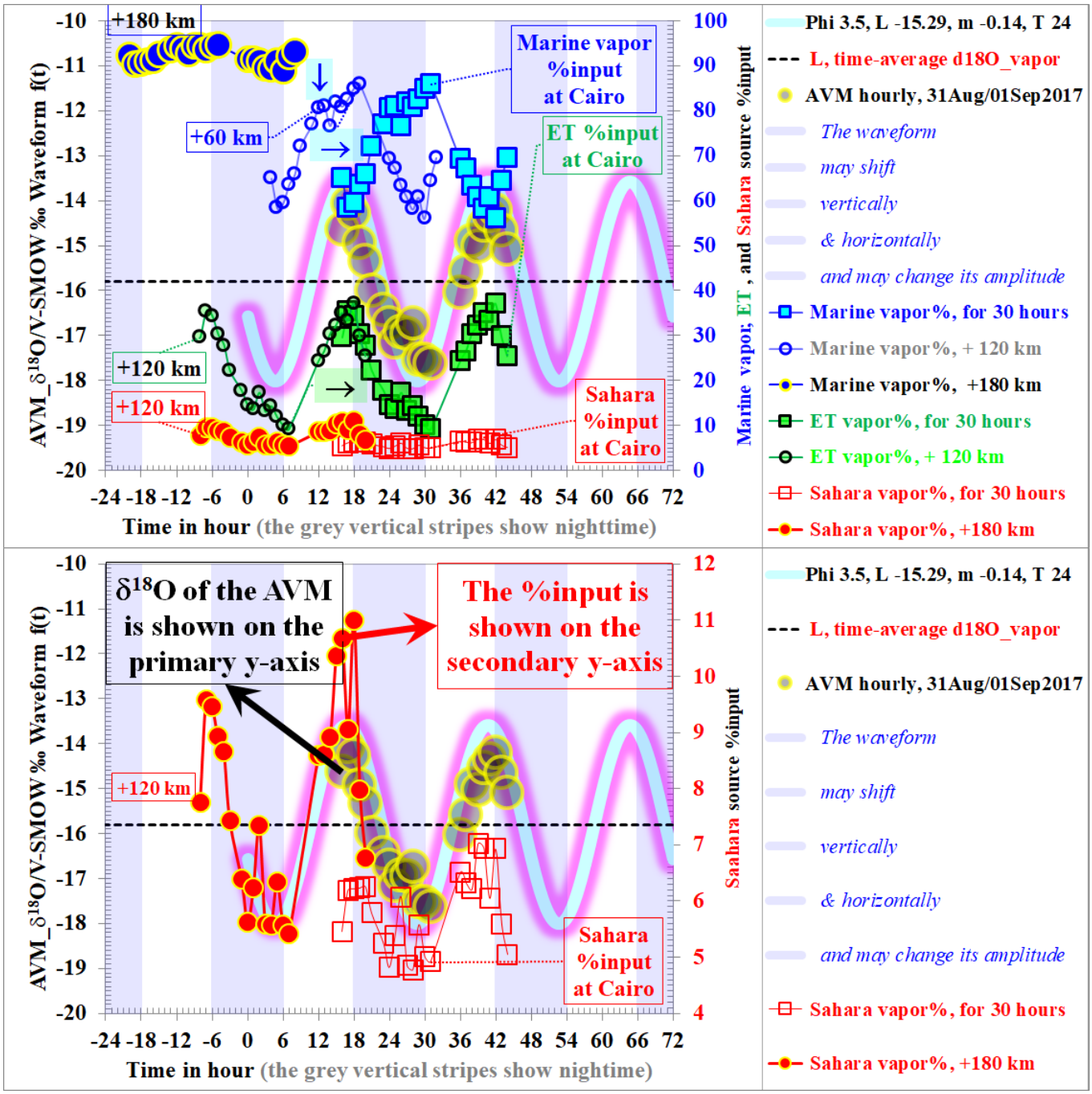

Figure 24

Time-controlled dynamics, for the change in the percent contributions of the three vapor sources making up the local AVM.

Supplementary Files

This is a list of supplementary files associated with this preprint. Click to download.

- Tables.docx